Analytical investigation of heat transfer enhancement in a channel partially filled with a porous material under local thermal non-equilibrium condition: effects of different thermal boundary conditions at the porous-fluid interface

Y. Mahmoudi*[1], N. Karimi[2], K. Mazaheri[3]

[1] *Department of Engineering, University of Cambridge, Cambridge, United Kingdom*

[2] *School of Engineering, University of Glasgow, Glasgow, United Kingdom*

[3] *Department of Mechanical Engineering, Tarbiat Modares University, Tehran, Iran*

** Corresponding author: Tel.: +44-7405247502; email: ymahmoudi@yahoo.com; sm2027@cam.ac.uk*

Abstract

Enhancement of forced convective heat transfer is analytically investigated in a channel partially filled with a porous medium under Local Thermal Non-Equilibrium (LTNE). Thermally and hydrodynamically fully developed conditions are considered. The flow inside the porous material is modelled by the Darcy-Brinkman-Forchheimer equation. The thermal boundary conditions at the interface between the porous medium and the clear region are described by two different models. For each interface model exact solutions are developed for the solid and fluid temperature fields. The Nusselt number (Nu) associated with each interface model is derived in terms of the porous insert normalised thickness (S) and other pertinent parameters such as thermal conductivity ratio (k), Biot number (Bi), and Darcy number (Da). The differences between the two interface models in predicting the temperature fields of the solid and fluid phases and validity of the Local Thermal Equilibrium (LTE) assumption are examined. Subsequently, for each model the values of S, Bi, k and Da at which LTE holds are determined. Further, the maximum values of S up to that the two models predict LTE condition are found as a function of Bi, k and Da. For each model and for different pertinent parameters the optimum value of S, which maximises the Nu number, is then found. The results show that, in general, the obtained Nu numbers can be strongly dependent upon the applied interface model. For large values of k and Bi, there are significant disparities

between the *Nu* numbers predicted by the two models. Nonetheless, for most values of *k* and *Bi*, and under different values of *Da* numbers both models predict similar trends of variation of *Nu* number versus *S*. The *Nu* number and pressure drop ratio are then used to determine the Heat Transfer Performance (HTP). It is found that for $S<0.9$ HTP is independent of *Da* number and the model used at the porous-fluid interface. For $S>0.9$, reduction of *Da* results in smaller values of HTP and signifies the difference between the values of HTP predicted by the two interface models.

Key words**:** Analytical solution, heat transfer enhancement, porous media, porous-fluid interface, local thermal non-equilibrium.

---

1. Introduction

Energy saving is of primary importance in the design of heat exchangers. This has severely intensified the demand for high performance heat exchangers [1]. Significant efforts are therefore being made to improve the performance of heat exchangers. It is now well known that heat convection can be enhanced through using porous material [2]. Convective heat transfer in porous media features a wide range of engineering applications, including those in oil recovery, geothermal engineering, chemical reactors, hydrogeology, heat pipes, solid matrix heat exchangers and thermal insulation. In most of these applications, it is preferred not to fully fill the system with the porous medium. This is to avoid the significant pressure drops occurring in the fully filled systems. Therefore, partial filling is an attractive way of enhancing heat transfer, while maintaining the pumping expense at a reasonable level [3-5].

A number of authors have studied heat transfer performance of different partially porous filled systems. Poulikakos and Kazmierczak [6] studied fully developed forced heat convection in a channel partially filled with a porous medium. In this study, the porous material was attached to the channel wall. They found that there is an extremum porous thickness at which Nusselt number is minimum. Another study showed that the thermal performance of a conventional concentric tube heat exchanger could be improved by inserting high thermal conductivity porous substrates [7]. The transient, developing, forced-convection flow in a concentric annuli partially filled with porous substrates was studied under two configurations [7]. These included the porous substrate attached either to the inner or outer cylinder [7]. In both cases, the boundary in contact with the porous substrate was exposed to a sudden change in its temperature while the other boundary was kept

adiabatic [7]. It was found that comparing to the clear pipe, porous substrates may improve the Nusselt number by the factor of twelve [7]. An investigation concentrated on the developing region of parallel-plate ducts, showed that when a porous substrate is attached to the inner wall of one plate, the Nusselt number is lower than that in a clear channel [8]. The highest Nusselt Number, under this condition, is achieved by the fully filled porous duct [8]. A study of forced convection in a pipe partially filled with porous substrates, with porous material inserted at the core of the pipe, revealed an order of magnitude increase in the Nusselt number compared to the clear pipe [4]. The numerical simulations [4] and experimental observations [9] showed that Nusselt number increases through partial filling, while the pressure drop is less than that of a conduit fully filled with a porous medium. Importantly, the configuration of the porous insert in the pipe can have a substantial effect on the rate of heat transfer [5]. It has been demonstrated numerically that if the porous material with low thermal conductivity is attached to the pipe inner wall, the Nusselt number is lower than that of the clear pipe [5]. However, under the same configuration and for the high values of thermal conductivity the obtained Nusselt number is always higher than its equivalent in the clear pipe [5]. The same study [5] reported that for different porous thermal conductivities inserting porous material at the core of the pipe results in the heat transfer rates much higher than those in the clear pipe [5].

It has been, recently, shown that inserting porous material in a channel could increase the Nusselt number up to 50% of that in a clear channel [10]. Further, in a partially filled parallel plate channel for the Darcy number of 10^{-3} the Nusselt number is maximum at the porous thickness ratio of 0.8 [10]. This ratio is defined as the thickness of the porous layer divided by the spacing between the two plates. Vafai and Kim [11] found that enhancement of heat transfer using porous material depends on the ratio of the effective thermal conductivity of the porous medium to that of the fluid. Darcy number, porous medium thickness, ratio of the effective thermal conductivity of the porous medium to that of the fluid and the configuration of the porous insert have been all found influential on the heat transfer rate [12-14]. A comprehensive review of the various aspects of the problem including dimensions, governing equations, outer surface thermal conditions and solution methods is given by Ref. [15]. Most works on convective heat transfer in porous media have assumed laminar fluid flow. Nonetheless, other flow regimes have been also studied numerically in the partially filled pipes [16, 17]. Assuming turbulent flows, it has been shown that to enhance heat transfer the optimum ratio of the porous medium thickness to pipe diameter is 0.8 [16, 17]. This value is very similar to that found in the laminar flows [3, 4].

All of the studies, cited so far, used the Local Thermal Equilibrium (LTE) model and argued that by using porous material heat transfer could be enhanced. In principle, there are two methods of modelling the energy equation in a porous medium. These include local thermal equilibrium (LTE) and local thermal non-equilibrium (LTNE) models [18]. LTE holds only when the temperature difference between the solid and fluid phases is negligibly small. In reality, however, this temperature difference may not be small. Hence, a more precise analysis should relax the assumption of LTE and use LTNE model instead. In a system partially filled with porous material there are two regions with different temperatures, namely the porous region and the fluid in the clear region. Therefore, the use of LTNE model at the porous-fluid interface requires additional information to account for the modes of energy communication between the two phases [19]. This information are usually provided in the form of porous-fluid interface models [19]. This, in turn, makes the thermal behaviour of the system dependent upon the applied interface model. Extra levels of complexity are, hence, added to the problem, which involve devising the proper interface models and including them in the analysis.

Boundary conditions and the physics of porous-fluid interface have been already subjected to detailed studies (e.g. [20]). In an analytical work, Vafai and Thiyagaraja [21] investigated the velocity and temperature fields at the interface region. They used the Brinkman-Forchheimer extended Darcy equation and considered three fundamental types of interface. These included the interfaces between two porous regions, a porous medium and a fluid layer and a porous medium and an impermeable medium. An exact solution for the fluid mechanics of the interface region between a porous medium and a fluid layer was put forward by Vafai and Kim [22]. This solution accounts for both boundary and inertial effects. When a heat flux is applied to the outer surface of a porous medium, the applied heat is transferred to the solid and fluid parts. The constant heat flux boundary condition could be viewed in two different ways [23]. The first is to assume that the heat division between the two phases is based on their effective conductivities and the corresponding temperature gradients. In the second approach, each of the two phases at the interface receives an equal amount of heat flux [23]. The first and second approaches in Ref. [23] later led to the introduction of two interface models, respectively referred to as models A and B [19]. Alazmi and Vafai [24] studied the effect of using different boundary conditions under constant wall heat flux and LTNE condition. Their study included six models based on the first approach and two models based on the second approach of Amiri et al. [23]. This work [24] revealed that either of the models could represent the boundary condition and the proper choice of the interface model is essentially problem dependent.

The first approach (model A) was, recently, used by Mahmoudi and Maerefat [3] to study the problem of forced convection in a channel partially filled with a porous medium [3]. Exact solutions were developed for both fluid and solid temperature fields in the porous and clear regions [3]. In this study Nusselt number was expressed as a function of porous insert thickness, porosity, thermal conductivity, Biot number and Darcy number [3]. It was shown that as the porous medium thickness increases, the error of using LTE model increases and the fully filled channel yields the maximum error [3]. Yang and Vafai [19] used Darcy-Brinkman model and analytically investigated the fully developed flow in a channel partially filled with a porous medium. These authors considered five forms of thermal boundary conditions at the interface between a porous medium and fluid under LTNE (based on the so-called models A, B and C [19]). They presented exact solutions for all of these conditions and further reported the restrictions in the validity of LTE in a partially filled system. The temperature gradient bifurcation in a channel filled with a porous medium, with internal heat generation was analysed by Yang and Vafai [25]. Under constant wall heat flux boundary condition exact solutions were obtained for the fluid and solid temperature distributions through two primary approaches to the interface. These included using models A and B according to the first and second approaches of Amiri et al. [23]. Most~~Very~~ recently, Mahmoudi and Karimi [26] studied numerically the heat transfer enhancement in a pipe partially filled with a porous medium under LTNE condition~~,~~. They ~~using two~~used two interface models A and B and ~~with the inclusion of~~ considered the inertia term (F). These authors~~y~~ [26] found that for a given interface model and for Darcy numbers less than 10^{-3}, the Nusselt number is independent of the inertia. ~~While~~ Nonetheless, for Darcy numbers higher than 10^{-3} as F increases, the Nusselt number also increases [26].

Validity of LTE has been also analytically examined for a thermally fully developed flow in a partially filled tube under constant wall heat flux [27]. It was shown that the local thermal equilibrium assumption might fail for the case of constant heat flux wall [27]. The validity of LTE in a partially filled pipe under two different configurations has been also studied analytically [28]. Local thermal equilibrium condition found to be invalid when the porous material is attached to the pipe wall. However, it was found out that LTE holds when the porous material is inserted at the core of the pipe [28]. Most recently, Vafai and Yang [29] highlighted the heat flux bifurcations at the porous-fluid interface as a fundamental problem with potentials of opening new research areas. In a separate work [18], Yang and Vafai investigated heat flux bifurcation inside a porous medium in a channel partially filled with a porous material and determined the validity range of LTE. The effects of thermal dispersion and inertia on the validity of LTE were further considered in their study.

The present review of literature shows that currently there exists a wealth of information gained by the various LTE analyses of the partially filled systems. LTNE analyses, however, are still being challenged by the sophisticated nature of the interface models, which can strongly affect the rest of the problem. It is essential to note that, so far, there has been no superior interface model [19, 24, 25, 29]. Determination of the proper thermal boundary condition at the porous-fluid interface is still an open question [19, 29]. Designating one model over the other is not a trivial task as some previous studies validated both of these primary models (models A and B [19]). Further, the mechanisms of splitting the heat flux between the two phases are not fully understood yet [19, 29] and different models have been validated experimentally for different sets of parameters [29]. Hence, choosing the proper interface model is, in general, heavily problem dependent [3, 19, 24]. As a result, slight modifications of the physical parameters of a given porous-fluid composite system can make a particular model preferable over the others [19]. Conversely, there exist some regions in the parametric space, in which different models are almost equally applicable and hence selection of the interface model is trivial. Significant simplifications might be applicable in these cases. Any set of parameters under which the LTE assumption holds, is an example of such situation [30, 31]. For instance, it has been shown that in a fully filled channel when the thermal conductivities of the fluid and solid phases are similar, the two phases are close to the local thermal equilibrium [32]. However, for different thermal conductivities of the fluid and solid phases, model B matches the experimental data [32]. In the study of Amiri et al. [23], good agreements were found between the numerical results using model B and the available experimental results. On the other hand, Hwang et al. [33] used the first approach and found good agreement between their numerical and experimental results. Another example can be a partially filled pipe with large heat transfer between the fluid and solid phases at the interface. In this case, temperatures of the two phases are equal at the interface and therefore model A is applicable. However, when the heat transfer between the fluid and solid phases at the interface is not strong enough the fluid and solid temperatures at the interface are not equal and model B is preferred. Furthermore, previous works have shown that depending on the thickness of the porous material and other pertinent parameters the fluid velocity in the clear region and at the interface changes [3]. This, in turn, changes heat transfer at the porous fluid interface. Thus, depending upon different parameters such as porous thickness, thermal conductivity ratio, Darcy number and inertial term either of models A or B can be applicable.

Due to these subtleties and complications, it is very useful to know the heat transfer behaviour of a partially filled system under varying parameters and interface models. This provides an

overview of the sensitivity of the problem upon the interface models as the pertinent physical parameters vary. It also illustrates the main similarities and distinctions between different interface models in predicting the heat transfer characteristics of the system [19, 25]. Hence, it highlights the regions in the parametric space in which the choice of the interface model is either critical or immaterial. In particular, it determines the validity limits of the LTE assumption under changing physical parameters and interface models. Most importantly, the use of a simple configuration facilitates understanding of the physical mechanisms responsible for the variations in the system behaviour. This physical understanding is central to the analysis of the more involved configurations found in engineering problems. It is the ultimate aim of this study to develop such understating through an analytical approach.

To this end, we consider the two most fundamental forms of the porous-fluid interface models [23] in a generic configuration of a partially porous-filled channel. In keeping with the literature, these two are regarded as model A and model B [25]. These models are applied to the investigated configuration and analytical solutions are developed for the temperature fields and Nusselt numbers. A series of parametric studies is then conducted. This is to gain physical insight into the behaviour of the system under varying physical parameters and interface models. The investigated parameters include Darcy and Biot numbers, thickness of the porous insert and solid to fluid conductivity ratio. An emphasis is first put on the detection of the regions in which the LTE holds. Then, the values of Nusselt number obtained by utilising different thermal interface models are compared and discussed. The developed analytical results, further, serve as a means of validation for the newly developed numerical tools and other theoretical studies.

Figure 1 is a schematic view of the problem under investigation. Fluid moves into a channel in which a porous material is sandwiched at the core of the channel. Constant wall heat flux boundary condition is considered at the channel wall. The height of the channel is h_0 and that of the porous material is h_p. Due to the symmetry of the configuration only half of the channel is considered in the analysis.

The configuration shown in Fig.1 is practically appealing. As explained earlier, two different partially filled configurations have been previously studied [5, 15]. These include centrally located porous material at the core of the pipe and an annulus porous material attached to the inner wall of a pipe [5, 15]. It was shown that in the first configuration, increasing the porous material thickness to a certain value increases the Nusselt number [5]. After exceeding a certain thickness, further increase in the thickness of the porous insert, results in the reduction of the Nusselt number [5]. However, a reversed trend is observed in the second configuration for low thermal conductivity of

the porous medium. Here, increasing the thickness of the porous insert first results in the reduction of the Nusselt number [5]. Upon reaching a critical value of the thickness the Nusselt number starts to grow [5]. Further, in the second configuration and for high thermal conductivity of the porous material, increasing the porous thickness increases the Nusselt number. In this configuration the fully filled configuration, yields the maximum Nusselt number [5]. This clearly shows that the configuration of the partially filled channels can either enhance or decrease the rate of heat transfer to the fluid. Since in the present work the purpose of adding porous insert is to enhance the heat transfer rate, the configuration shown in Fig. 1 was chosen. This configuration has also been considered in a number of previous investigations, e.g. [3-5, 9, 18, 19, 34], under LTE condition. These studies had different objectives to those of the current study. Nonetheless, some general features of the selected configuration, such as hydrodynamics, are well documented in them. This provides a viable setting for understating of the observed physical behaviours.

The following assumptions are made throughout this study [3, 18, 19, 25, 30, 31]. These, along with the configuration shown in Fig. 1 constitute a porous-fluid system suitable for the purposes of our study while keeping the problem amenable to an analytical approach.

- The porous medium is homogenous, isotropic and saturated with the fluid.
- The flow is laminar, steady and incompressible, with no gravity effects.
- Thermally and hydrodynamically fully developed conditions hold in the entire clear and porous regions.
- Natural convection, radiation heat transfer, and viscous heat generation are negligible.
- Physical properties such as porosity, specific heat, density and thermal conductivity are constant. Since the thermal conductivity is assumed constant the effects of thermal dispersion [35, 36] are ignored here.

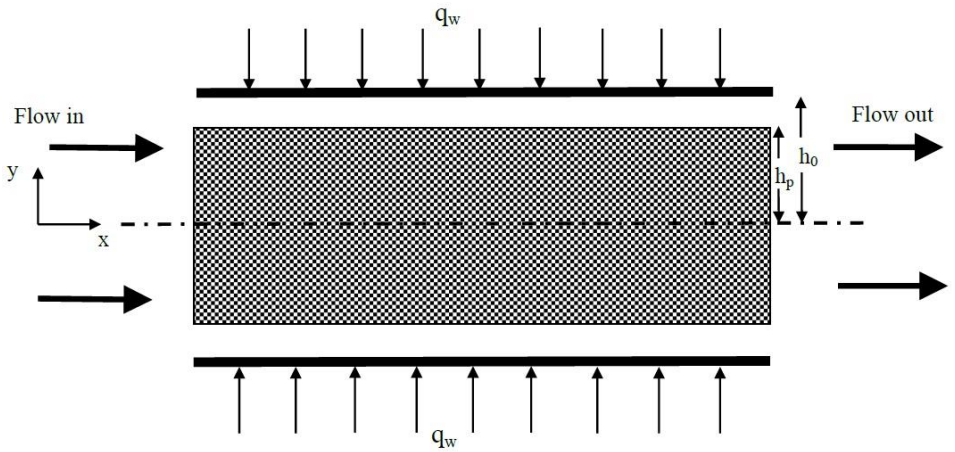

Fig. 1. Schematic of the investigated configuration.

The current investigation aims at the followings specific targets.

- Development of exact solutions for the temperature profile of the fluid and solid phases in the porous region by using two different interface models (models A and B),
- development of an exact solution for Nusselt number as a function of porous material thickness, thermal conductivity, Biot number and Darcy number,
- comparison of models A and B predictions of heat flux distribution as a function of porous thickness and Darcy number,
- finding under which conditions the two interface models predict the same results, or there is no need for interface models at all i.e. LTE holds.
- determining from which point in the parametric space, the two models deviate from each other and how significant this deviation is.
- exploring the physical mechanisms responsible for varying the behaviour of the system as the pertinent parameters of the system change.
- determination of an optimum porous material thickness up to that LTE holds for different interface models and varying thermal conductivities, Darcy and Biot numbers,
- determination of an optimum porous material thickness up to that the two models predict similar temperatures for the solid and fluid phases,
- determination of the value of porous thickness which yields the maximum Nusselt number for each interface model and for varying Darcy number, thermal conductivity and Biot number,
- presenting a discussion on the differences between models A and B in predicting the heat transfer performance (HTP) of the system.

The remaining of this paper is organised as follows. The analytical methods including governing equations, boundary conditions and dimensionless variables are explained in section 2. The analytical solutions for the temperatures and Nusselt numbers are further presented in this section. Section 3 includes discussions of the obtained results and section 4 concludes the paper.

2. Analytical methods

2.1. Governing equations

For the thermally and hydrodynamically developed region and by ignoring natural convection and radiation heat transfer, the governing equations of the fluid flow and heat transfer are reduced to the following relations [3, 19, 27]. Momentum equation in the clear region is expressed by

$$-\frac{\partial p}{\partial x}+\mu\frac{\partial^2 u_f}{\partial y^2}=0. \tag{1}$$

Previous investigations [3, 4, 9] have shown that within the porous medium and for $Da<10^{-3}$, the inertia term of the momentum equation is negligible. Further, Darcy flow model is restricted to the flows in which the viscous forces dominate over the inertia forces and therefore Reynolds number based on the mean pore diameter does not exceed unity [2]. Thus, Darcy-Brinkman model can be used in this region and the momentum equation in the porous medium becomes

$$-\frac{\partial p}{\partial x}+\mu_{eff}\frac{\partial^2 u_p}{\partial y^2}-\frac{\mu}{K}u_p=0. \tag{2}$$

Energy equation for the fluid in the clear region is expressed as

$$\rho c_p u_f\frac{\partial T_{f1}}{\partial x}=k_f\frac{\partial^2 T_{f1}}{\partial y^2}. \tag{3}$$

Fluid phase energy equation in the porous region yields

$$\rho c_p u_p\frac{\partial T_{f2}}{\partial x}=k_{f,eff}\frac{\partial^2 T_{f2}}{\partial y^2}+a_{sf}h_{sf}\left(T_s-T_{f2}\right), \tag{4}$$

and solid phase energy equation in the porous region is written as

$$0=k_{s,eff}\frac{\partial^2 T_s}{\partial y^2}-a_{sf}h_{sf}(T_s-T_{f2}), \tag{5}$$

where, $k_{f,eff}$ and $k_{s,eff}$ are respectively the effective thermal conductivity of the fluid phase and the solid phase.

2.2. Boundary conditions

The boundary conditions for the momentum equations are

$$u_f=0 \qquad at \quad y=\mathrm{h}_0, \tag{6}$$

$$u_f=u_p,\ \mu_f\frac{\partial u_f}{\partial y}=\mu_{eff}\frac{\partial u_p}{\partial y} \qquad at \quad y=\mathrm{h}_\mathrm{p}, \tag{7}$$

$$\frac{\partial u_p}{\partial y}=0 \qquad at \quad y=0, \tag{8}$$

and those of the energy equations include

$$\frac{\partial T_{f2}}{\partial y} = \frac{\partial T_s}{\partial y} = 0, \qquad at \quad y = 0, \tag{9}$$

$$k_f \frac{\partial T_{f1}}{\partial y} = q_w \quad , \quad at \quad y = \mathrm{h}_0, \tag{10}$$

$$T_{f1} = T_{f2}, \qquad at \quad y = \mathrm{h}_\mathrm{p}, \tag{11}$$

in which subscripts f_1 and f_2 respectively denote the fluid phase in the clear region and the porous medium. In the above equations, μ_{eff} is the effective viscosity of the fluid inside the porous medium. This is an artificial quantity associated with the Brinkman term in the momentum equation [37]. In general, the effective viscosity is not only a function of the porosity and also strongly depends on the geometrical structure of a porous medium [37]. However, it has been shown [38] that the results obtained by assuming $\mu_{eff} = \mu_f$ are in good agreement with the experimental and numerical results of Ref. [39]. Alazmi and Vafai [29] showed that changing μ_{eff} from μ_f to 7.5 μ_f has a minor influence on the velocity profile. In addition, they reported that the effect of changing effective viscosity has a minor influence on the temperature and Nusselt number distributions [29]. Hence, the same assumption is made throughout this study. Equation (7) states the continuity of the fluid velocity and a balance of shear stress on the interface through using the effective viscosity μ_{eff}, [3, 5, 21, 40].

In order to close the system of governing equations and solve the equations analytically, the thermal boundary condition at the porous-fluid interface should be specified. In the present work, two models (model A and B of Yang and Vafai [25] and/or model 1A and model 2A of Alazmi and Vafai [24]) are utilised to describe the temperature at the interface between the clear and porous regions [3, 24, 25]. In the work of Mahmoudi and Maerefat [3] they considered model A at the porous-fluid interface and obtained analytical solutions for the temperature field and Nusselt number. Here, two primary model A and model B under LTNE condition are analysed, leading to a presentation of exact solutions for temperature field and Nusselt number under two models. This leads to the development of exact solutions for the temperature fields and Nusselt numbers. The work concentrates on the effect of the interface models upon the critical values of porous thickness for validity of LTE and optimum porous thickness for heat transfer enhancement.

Model A assumes that heat is divided between the two phases on the basis of their effective conductivities and their corresponding temperature gradients [3, 19] and therefore

$$q_{\text{interface}} = k_{f,eff} \left.\frac{\partial T_f}{\partial y}\right|_{\text{interface}} + k_{s,eff} \left.\frac{\partial T_s}{\partial y}\right|_{\text{interface}}, \tag{12a}$$

$$T_f\Big|_{\text{interface}} = T_s\Big|_{\text{interface}} = T_{\text{interface}}. \tag{12b}$$

Model B, however, assumes that both phases at the interface receive the same amount of heat flux [3, 19, 25]. Hence,

$$k_{f,eff}\left.\frac{\partial T_f}{\partial y}\right|_{\text{interface}} = k_{s,eff}\left.\frac{\partial T_s}{\partial y}\right|_{\text{interface}} = q_{\text{interface}}. \tag{13}$$

In Eqs. (12) and (13) $q_{\text{interface}} = k_f \left.\frac{\partial T_{f1}}{\partial y}\right|_{y=\text{h}_\text{p}}$ and $T_{\text{interface}}$ denotes the heat flux and the temperature at the porous-fluid interface. It should be noted that Eq. (12b) is a part of model A. It requires temperatures of the two phases to be locally equal only on the porous-fluid interface. This is different to the local thermal equilibrium (LTE) assumption, in which the temperatures of the two phases are deemed the same at any local point within the porous region [31 ,30 ,26-23]. The average flow velocity in the channel is [3]

$$\bar{u} = \frac{1}{\text{h}_0}\left[\int_0^{\text{h}_\text{p}} u_p dy + \int_{\text{h}_\text{p}}^{\text{h}_0} u_f dy\right]. \tag{14}$$

In order to solve the energy equations (3) and (4) the left hand side of these equations needs to be determined. Consequently, the amount of heat flux at the porous-fluid interface, $q_{\text{interface}}$ can be obtained. Integrating Eq. (3) from h_p to h_0 and noting that in the fully developed region $\frac{\partial T_{f1}}{\partial x} = \frac{\partial T_{f2}}{\partial x} = \frac{\partial T_f}{\partial x} = \text{const}$, result in

$$\rho c_p \frac{\partial T_f}{\partial x}\int_{\text{h}_\text{p}}^{\text{h}_0} u_f dy = (q_w - q_{\text{interface}}). \tag{15}$$

Adding Eqs. (4) and (5) and integrating the sum from 0 to h_p and applying the boundary conditions given by Eq. (12) reveals

$$\rho c_p \frac{\partial T_f}{\partial x}\int_0^{\text{h}_\text{p}} u_p dy = q_{\text{interface}}. \tag{16}$$

Adding Eq. (15) to Eq. (16) and using Eq. (14) yields

$$\rho c_p \left.\frac{\partial T_f}{\partial x}\right|_{\text{Model A}} = \frac{q_\text{w}}{\text{h}_0}\frac{1}{\bar{u}}. \tag{17}$$

Substituting Eq. (17) into Eq. (16) gives model A prediction of the heat flux at the porous medium-fluid interface as [3],

$$\left.\frac{q_{\text{interface}}}{q_w}\right|_{\text{ModelA}} = \frac{1}{\mathrm{h}_0\bar{u}}\int_0^{\mathrm{h_p}} u_p\, dy. \tag{18}$$

By adding Eqs. (4) to (5) and integrating the sum from 0 to $\mathrm{h_p}$ and applying boundary condition (13) (model B) the following equation is obtained,

$$\rho c_p \frac{\partial T_f}{\partial x}\int_0^{\mathrm{h_p}} u_p dy = 2q_{\text{interface}}. \tag{19}$$

Adding Eq. (15) to Eq. (19) and incorporating Eq. (14) result in

$$\left.\rho c_p \frac{\partial T_f}{\partial x}\right|_{\text{ModelB}} = \frac{1}{\mathrm{h}_0\bar{u}}\left(q_w + q_{\text{interface}}\right). \tag{20}$$

Similarly substituting Eq. (20) into Eq. (19) reveals model B prediction of heat flux at the porous medium-fluid interface, which is

$$\left.\frac{q_{\text{interface}}}{q_w}\right|_{\text{ModelB}} = \frac{\int_0^{\mathrm{h_p}} u_p \mathrm{d}y}{2\mathrm{h}_0\bar{u} - \int_0^{\mathrm{h_p}} u_p \mathrm{d}y}. \tag{21}$$

A physical description can be given for Eq. (19). The heat flux $q_{\text{interface}}$ from the outer surface is transferred to the porous medium through two different ways. The first part of heat is transferred through conduction in the fluid phase, q_f , and the rest is by conduction in the solid phase, q_s [31]. Based on model B, each phase receives the same amount of heat flux, which is equal to $q_{interface}$. That is $q_f = q_{interface}$ and $q_s = q_{interface}$. This methodology is consistent with the second approach of Amiri et al. [23]. The heat transferred to the solid phase is ultimately transferred to the fluid phase through an internal heat exchange process [31]. Consequently, the total internal heat exchange equals the total heat transferred from the wall to the solid phase via solid conduction [31]. That is $q_{exch} = q_s$. Thus, the overall heat transfer to the fluid phase is partly by direct conduction into the fluid and partly by conduction through the solid and subsequent internal heat exchange from the solid to the fluid [31]. This reveals that the total heat flux delivered to the fluid in the porous region is $q_{total,fluid,porous} = q_f + q_{exch}$. Further, since $q_{exch} = q_s$, it follows that $q_{total,fluid,porous} = q_f + q_s$. The definition of model B then requires $q_{total,fluid,porous} = q_{interface} + q_{interface} = 2\, q_{interface}$. It is noted that the previous applications of model B, in the fully filled configurations, have led to similar results [25].

2.3. Normalised quantities and velocity profiles

The problem formulated so far, includes a large number of variables. To reduce the number of these variables and provide further physical insight a normalisation process is introduced here. To normalise the governing equations and boundary conditions the following dimensionless variables are introduced.

$$\Theta\big|_{\text{ModelA}} = \frac{k_{s,eff}\left(T - T_{\text{interface}}\right)}{q_{\text{w}}\,\text{h}_0}, \tag{22a}$$

$$\Theta\big|_{\text{ModelB}} = \frac{k_{s,eff}\left(T - T_{\text{s,interface}}\right)}{q_{\text{w}}\,\text{h}_0}, \tag{22b}$$

$$\gamma = \frac{q_{\text{interface}}}{q_{\text{w}}}, \tag{22c}$$

$$k = \frac{k_{s,eff}}{k_{f,eff}}, \tag{22d}$$

$$Bi = \frac{a_{sf} h_{sf} \text{h}_0^2}{k_{s,eff}}, \tag{22e}$$

$$Y = \frac{y}{\text{h}_0}, \tag{22f}$$

$$S = \frac{\text{h}_\text{p}}{\text{h}_0}, \tag{22g}$$

$$U = \frac{u}{u_r}, \tag{22h}$$

where u_r is a characteristic velocity defined as $u_r = -\frac{\text{h}_0^{\,2}}{\mu}\frac{\partial p}{\partial x}$. Equation (12) states that, under model A, the temperature of the fluid phase and solid phase are the same and equal to the interface temperature. However, according to model B (Eq. (13)) the fluid and solid temperatures are not identical. In relation (22e) *Bi* is the Biot number, which represents the ratio of the solid phase conduction resistance to that against the heat exchange between the two phases [3, 19, 31]. The ratio of the effective thermal conductivity of the solid to that of the fluid is denoted by *k*. Further, γ is the ratio of the wall heat flux to the flux transported from the clear region to the porous medium. More details on the normalisation of the governing equations and the boundary conditions can be found in Ref. [3].

Hydrodynamics of the present problem have been solved previously [3, 41]. It has been shown that the solutions for the momentum Eqs. (1) and (2) and the corresponding boundary conditions (6), (7), and (8) are as follows [3, 41]. In the clear region,

$$U_f(Y) = -\frac{1}{2}Y^2 + AY + B, \tag{23}$$

$$A = S + \frac{Z\sinh(ZS)(S - 0.5\times(1+S^2) + Da)}{Z(S-1)\sinh(ZS) - \cosh(ZS)}, \tag{24}$$

$$B = 1/2 - S - \frac{Z\sinh(ZS)(S - 0.5\times(1+S^2) + Da)}{Z(S-1)\sinh(ZS) - \cosh(ZS)}. \tag{25}$$

Within the porous region,

$$U_p = C\cosh(Z\,Y) + Da\ , \tag{26}$$

$$C = \frac{1}{Z\sinh(ZS)} \times (A - S). \tag{27}$$

Using Eqs. (23) and (26) and dimensionless parameters in (22) the dimensionless average velocity presented in Eq. (14) becomes

$$\overline{U} = SDa + \frac{D}{Z}\sinh(ZS) - \frac{1}{6}(1-S^3) + \frac{1}{2}A(1-S^2) + B(1-S), \tag{28}$$

where $Z = \sqrt{1/Da}$. Further, S is the ratio of the porous medium thickness to the channel height (Eq. (22g)) and A, B and C are respectively defined in Eqs. (24), (25) and (27). These hydrodynamic fields are later used in the solution of the heat flux at the porous-fluid interface and the energy equations.

The dimensionless form of Eq. (18) gives the amount of heat flux at the porous-fluid interface for model A. This is,

$$\gamma\big|_{\text{Model A}} = \frac{1}{\overline{U}}\int_0^s U_p\, dY. \tag{29}$$

Equations (26) and (28) can be combined to show

$$\gamma\big|_{\text{Model A}} = \frac{\frac{D}{Z}\sinh(ZS) + SDa}{SDa + \frac{D}{Z}\sinh(ZS) - \frac{1}{6}(1-S^3) + \frac{1}{2}A(1-S^2) + B(1-S)}. \tag{30}$$

Similar to that explained in the derivation of Eq. (29), the dimensionless form of Eq. (21) is employed to obtain an expression for the heat flux at the porous-fluid interface under model B. This results in

$$\gamma\big|_{\text{Model B}} = \frac{\int_0^s U_p\, dY}{2\overline{U} - \int_0^s U_p\, dY}. \tag{31}$$

Once again by using Eqs. (26) and (28) it can be shown that

$$\gamma\big|_{\text{Model B}} = \frac{\frac{D}{Z}\sinh(ZS) + SDa}{2(SDa + \frac{D}{Z}\sinh(ZS) - \frac{1}{6}(1-S^3) + \frac{1}{2}A(1-S^2) + B(1-S)) - \frac{D}{Z}\sinh(ZS) + SDa}. \tag{32}$$

2.4 Solid and fluid temperature fields

The energy equations (4) and (5) are now solved using the two interface models. This reveals the temperature profiles of the fluid in the porous and clear regions as well as that of the solid matrix. These profiles are of physical significance and are also used in the rest of the analysis.

2.4.1. Temperature profile for model A

The energy equations and the associated boundary conditions are first derived through substitution of Eq. (22a) into Eqs. (3), (4) and (5). This reveals the energy equation for the fluid in the clear region as

$$\varepsilon k \frac{U_f}{\overline{U}} = \Theta''_{f1}(Y). \tag{33}$$

Fluid phase energy equation in the porous region takes the form of

$$\frac{U_p}{\overline{U}} = \frac{1}{k}\Theta''_{f2}(Y) + Bi\left(\Theta_s(Y) - \Theta_{f2}(Y)\right), \tag{34}$$

and the solid phase energy equation in the porous region can be written as

$$0 = \Theta''_s(Y) - Bi(\Theta_s(Y) - \Theta_{f2}(Y)). \tag{35}$$

The associated energy boundary conditions are

$$\Theta'_{f1}(1) = \varepsilon k, \tag{36}$$

$$\Theta_{f1}(S) = \Theta_{f2}(S) = \Theta_s(S) = 0, \tag{37a}$$

$$\Theta'_{f2}(0) = \Theta'_s(0) = 0. \tag{37b}$$

By taking the second derivative with respect to *Y*, the two coupled differential Eqs. (34) and (35) are manipulated to yield a new set of fourth order ordinary differential equations:

$$\Theta''''_{f2}(Y) - Bi(1+k)\Theta''_{f2}(Y) = \frac{k}{\overline{U}}(-BiU_p(Y) + U''_p(Y)), \tag{38}$$

$$\Theta''_s(Y) - Bi(1+k)\Theta''_s(Y) = -\frac{k}{\overline{U}} BiU_p(Y). \tag{39}$$

These two ordinary differential equations can be easily solved by using the appropriate boundary conditions. This results in the development of exact solutions for the temperature profiles of the fluid and solid phases within the porous region.

Evaluating the second and third derivatives of Θ_s and Θ_{f2} at *Y*=0 and *Y*=*S* by substituting Eqs. (37a) and (37b) into Eqs. (34) and (35) yields [3, 19, 30, 31],

$$\Theta''_{f2}(S) = k\frac{U_p(S)}{\overline{U}}, \qquad \Theta''_s(S) = 0, \qquad \Theta'''_{f2}(0) = 0, \qquad \Theta''_s(0) = 0. \tag{40}$$

Integrating the ordinary differential Eq. (33) gives the following expression for the temperature distribution of the flow in the clear region

$$\begin{aligned}\Theta_{f1}(Y)\big|_{\text{Model A}} = \frac{\varepsilon k}{\overline{U}}\Big(&-\frac{Y^4}{24} + A\frac{Y^3}{6} + B\frac{Y^2}{2} + \Big(\frac{1}{6} - \frac{A}{2} - B + \overline{U}\Big)Y + \frac{S^4}{24} - A\frac{S^3}{6} \\ &- B\frac{S^2}{2} - S\left[\frac{1}{6} - \frac{A}{2} - B + \overline{U}\right]\Big),\end{aligned} \tag{41}$$

where A and B are given by Eqs. (24) and (25). The temperature distributions in the porous region are found through solving Eqs. (38) and (39) using the boundary conditions given by Eqs. (37) and (40). This reveals

$$\Theta_{f2}(Y)\big|_{\text{Model A}} = \frac{k}{\overline{U}}\left\{\frac{C(Z^2 - Bi)\times[\cosh(ZY) - \cosh(ZS)\times(1+\xi\times Z^2)]}{Z^2(-\Gamma^2 + Z^2)} + \frac{Da\,Bi}{\Gamma^2}\times\left(-\xi + \frac{Y^2}{2} - \frac{S^2}{2}\right) + U_p(S)\xi\right\}, \tag{42}$$

$$\Theta_s(Y)\big|_{\text{Model A}} = -Bi\,\frac{k}{\overline{U}}\left\{\frac{C[\cosh(ZY) - \cosh(ZS)\times(1+\xi\times Z^2)]}{Z^2(-\Gamma^2 + Z^2)} - \frac{Da}{\Gamma^2}\left(-\xi + \frac{Y^2}{2} - \frac{S^2}{2}\right)\right\}, \tag{43}$$

where $\Gamma = \sqrt{Bi(1+k)}$ and $\xi = \left(\frac{\cosh(\Gamma Y)}{\cosh(\Gamma S)} - 1\right)\Big/\Gamma^2$.

The temperature distributions of the fluid and solid phases given by Eqs.(42) and (43) are similar to those obtained previously by Mahmoudi and Maerefat [3].

2.4.2. Temperature profile for model B

As it is mentioned in section 1, the main emphasize in the present work is to analyse two primary thermal boundary conditions at the porous-fluid interface on rate of heat transfer in a porous fluid composite system. Hence, in this section, the temperature profiles of the fluid and solid phases under model B are determined. Substitution of Eq. (22b) into Eqs. (3), (4) and (5) reveals the different forms of the energy equation applied to the two phases. Energy equation for the fluid in the clear region becomes

$$\varepsilon\, k(1+\gamma)\frac{U_f}{\overline{U}} = \Theta''_{f1}(Y), \tag{44}$$

and the fluid phase energy equation in the porous region takes the form of

$$\frac{U_p}{\overline{U}} = \frac{1}{k}\Theta''_{f2}(Y) + Bi\left(\Theta_s(Y) - \Theta_{f2}(Y)\right), \tag{45}$$

while solid phase energy equation in the porous region can be written as

$$0 = \Theta''_s(Y) - Bi(\Theta_s(Y) - \Theta_{f2}(Y)). \tag{46}$$

The associated energy boundary conditions are

$$\Theta'_{f1}(1) = \varepsilon k, \tag{47a}$$

$$\Theta_{f1}(S) = \Theta_{f2}(S), \tag{47b}$$

$$\Theta'_{f2}(0) = \Theta'_s(0) = 0, \tag{47c}$$

$$\Theta'_{f2}(s) = \gamma k, \tag{47d}$$

$$\Theta_s'(s)=\gamma, \tag{47e}$$

$$\Theta_s''(s)+Bi\,\Theta_{f2}(s)=0, \tag{47f}$$

$$\Theta_s(s)=0. \tag{47g}$$

Taking the second derivative of Eqs. (45) and (46) with respect to *Y* yields,

$$\Theta_{f2}''''(Y)-Bi(1+k)\Theta_{f2}''(Y)=\frac{k}{\overline{U}}(1+\gamma)(-BiU_p(Y)+U_p''(Y)), \tag{48}$$

$$\Theta_s''(Y)-Bi(1+k)\Theta_s''(Y)=-\frac{k}{\overline{U}}(1+\gamma)BiU_p(Y). \tag{49}$$

Ordinary differential equations (48) and (49) are now used to determine the temperature profiles of the fluid and solid phases. The second and third derivatives of Θ_s and Θ_{f2} at the symmetry plane (*Y*=0) are evaluated by applying Eq. (47), which renders

$$\Theta_{f2}'''(0)=k\frac{U_p'(0)}{\overline{U}}=0, \tag{50a}$$

$$\Theta_s''(0)=0. \tag{50b}$$

Finally, solving the ordinary differential Eq. (44) results in the following expressions for the temperature distribution of the flow in the clear region

$$\Theta_{f1}(Y)\big|_{\text{ModelB}}=\varepsilon\psi\left(-\frac{1}{24}Y^4+A\frac{Y^3}{6}+B\frac{Y^2}{2}+O_1Y+O_2\right), \tag{51a}$$

$$O_1=\frac{k}{\psi}-\left(-\frac{1}{6}+\frac{A}{2}+B\right), \tag{51b}$$

$$O_2=\frac{\Theta_{f2}(s)}{\varepsilon\psi}-\left(-\frac{1}{24}S^4+A\frac{S^3}{6}+B\frac{S^2}{2}+O_1S\right), \tag{51c}$$

where $\psi=\frac{k}{\overline{U}}(1+\gamma)$, *A* and *B* are respectively given by Eqs. (24) and (25). The temperature distributions in the porous region are found by solving Eqs. (48) and (49) and applying the boundary conditions (47) and (50). This results in the followings,

$$\Theta_{f2}(Y)\big|_{\text{ModelB}}=\frac{\phi 1}{\Gamma^2}\cosh(\Gamma Y)+\frac{Bi\,Da\psi}{\Gamma^2}\frac{Y^2}{2}-\frac{C\psi(Z^2-Bi)}{Z^2(Z^2-\Gamma^2)}\cosh(ZY)+\phi 2, \tag{52}$$

$$\begin{aligned}\Theta_s(Y)\big|_{\text{ModelB}}=&\frac{\phi 3}{\Gamma^2}\left[\cosh(\Gamma Y)-\cosh(\Gamma S)\right]+\frac{Bi\,Da\psi}{\Gamma^2}\left[\frac{Y^2}{2}-\frac{S^2}{2}\right]-\\&\frac{Bi\,C\psi}{Z^2(Z^2-\Gamma^2)}\left[\cosh(ZY)-\cosh(ZS)\right],\end{aligned} \tag{53}$$

where

$$\varphi 1=\frac{\Gamma}{\sinh(\Gamma S)}\left[\gamma k-\frac{BiDa\psi}{\Gamma^2}S-\frac{C\psi(Z^2-Bi)}{Z(Z^2-\Gamma^2)}\sinh(ZS)\right], \tag{54b}$$

$$\varphi 2=\frac{\Gamma}{\sinh(\Gamma S)}\left[\gamma-\frac{BiDa\psi}{\Gamma^2}S+\frac{Bi\,C\psi}{Z(Z^2-\Gamma^2)}\sinh(ZS)\right], \tag{54c}$$

$$\phi 3 = \cosh(\Gamma S)\left[-\frac{\phi 1}{\Gamma^2} - \frac{\phi 2}{Bi}\right] + \frac{BiDa\,\psi}{\Gamma^2}\left(-\frac{1}{Bi} - \frac{S^2}{2}\right) + \frac{BiC\,\psi}{Z^2(Z^2-\Gamma^2)}\cosh(ZS), \tag{54d}$$

$$\psi = \frac{k}{\overline{U}}(1+\gamma), \qquad \Gamma = \sqrt{Bi\,(1+k)}. \tag{54e}$$

in which A, B and C are given by Eqs. (24), (25) and (27).

2.5. Nusselt number

Nusselt number at the channel wall for S<1 (partial filling) is given by [42]

$$Nu = \frac{q_w D_h}{k_f (T_w - T_m)}. \tag{55}$$

For the fully filled channel (S=1) [43], it becomes

$$Nu = \frac{q_w D_h}{k_{f,eff} (T_w - T_m)}, \tag{56}$$

where D_h is the hydraulic diameter of the channel equal to $4h_0$. The right-hand side of Eq. (55) can be written in terms of the normalised parameters. For S<1 this provides

$$Nu = \frac{4\varepsilon k}{\Theta_w - \Theta_m}, \tag{57}$$

and for S=1 gives

$$Nu = \frac{4k}{\Theta_w - \Theta_m}, \tag{58}$$

where

$$\Theta_w = \Theta_{f1}\big|_{Y=1}. \tag{59}$$

The solutions, developed in section 2.4, for the temperature profiles are subsequently used to evaluate the right-hand side of relation (57). The obtained Nusselt numbers are expressed in terms of the pertinent dimensionless quantities. In particular, in order to analyse the effect of different thermal boundary condition at the porous-fluid interface on the rate of heat transfer, separate expressions are developed for the Nusselt numbers based on models A and B.

2.5.1. Nusselt number for model A

Using the definition of Nusselt number presented by Eq. (57) and utilising the expressions developed in section 2.4.1 the Nusselt number based on model A is derived here. Setting Y=1 in Eq. (41) model A reveals the non-dimensional temperature for the fluid at the channel wall as [3]

$$\Theta_w\big|_{\text{Model A}} = \frac{\varepsilon k}{\overline{U}}\left(\frac{1}{8} - \frac{A}{3} - \frac{B}{2} + \overline{U} + \frac{S^4}{24} - A\frac{S^3}{6} - B\frac{S^2}{2} - S\left[\frac{1}{6} - \frac{A}{2} - B + \overline{U}\right]\right), \tag{60}$$

in which A, B and $\overline{U}$ are respectively given by Eqs. (24), (25) and (28). The non-dimensional mean temperature is defined as

$$\Theta_m = \frac{\int_0^S U_p \Theta_{f2} dY + \int_S^1 U_f \Theta_{f1} dY}{\overline{U}}. \tag{61}$$

Through some algebraic manipulations, it can be shown that

$$\Theta_m\big|_{\text{Model A}} = I_A + II_A + III_A + IV_A, \tag{62a}$$

where

$$I_A = \frac{kC(Z^2 - Bi)}{\overline{U}^2 Z^2(-\Gamma^2 + Z^2)}\left\{Da\times\left[\frac{\sinh(ZS)}{Z} - \frac{\cosh(ZS)}{\Gamma^2}\times(\Gamma^2 S + Z^2(\frac{\tanh(\Gamma S)}{\Gamma} - S))\right]\right.$$

$$+C\times\left[\frac{S}{2} + \frac{\sinh(2ZS)}{4Z} - \cosh(ZS)\times\left\{\frac{\sinh(ZS)}{Z} + \frac{Z^2}{\Gamma^2}\times\right.\right. \tag{62b}$$

$$\left.\left.\left.\left(\frac{-\sinh(ZS)}{Z} + \frac{1}{\cosh(ZS)}\times(\frac{\sinh((Z+\Gamma)S)}{Z+\Gamma} + \frac{\sinh((\Gamma - Z)S)}{\Gamma - Z})\right)\right\}\right]\right\},$$

$$II_A = \frac{kDaBi}{\overline{U}^2\Gamma^2}\left\{\frac{CS}{Z^2}\times\left(\cosh(ZS) + \frac{S^2 Da}{2}\right) - \frac{C\sinh(ZS)}{Z^3} + \frac{S^3 Da}{6} + \frac{S^2}{2}\right.$$

$$\left. + \frac{1}{\Gamma^2}\times\left[\frac{C\sinh(ZS)}{Z} + SDa - \frac{C}{\cosh(\Gamma S)}\times(\frac{\sinh((Z+\Gamma)S)}{Z+\Gamma} + \frac{\sinh((Z-\Gamma)S)}{Z-\Gamma}) + \frac{Da\sinh(\Gamma S)}{\lambda\cosh(\Gamma S)}\right]\right\}, \tag{62c}$$

$$III_A = \frac{kU_p(S)}{\Gamma^2\overline{U}^2}\left\{\frac{C}{\cosh(\Gamma S)}\times\left[\frac{\sinh((Z+\Gamma)S)}{Z+\Gamma} + \frac{\sinh((Z-\Gamma)S)}{Z-\Gamma}\right]\right.$$

$$\left. - \frac{C\sinh(ZS)}{Z} + Da\times\left(\frac{\tanh(\Gamma S)}{\Gamma} - S\right)\right\}, \tag{62d}$$

and

$$IV_A = \frac{\varepsilon k}{\overline{U}^2}\left\{\frac{1}{336}\times(1-S^7) + \frac{-A}{48}\times(1-S^6) + \left(-\frac{A}{30} - \frac{7B}{120}\right)\times(1-S^5)\right.$$

$$+\left(\frac{AB}{6} - \frac{1}{8}\times(\frac{1}{6} - \frac{A}{2} - B + \overline{U})\right)\times(1-S^4) + (\frac{B^2}{6} + \frac{A}{3}\times(\frac{1}{6} - \frac{A}{2} - B + \overline{U}) - \frac{1}{6}\times$$

$$(\frac{S^4}{24} - A\frac{S^3}{6} - B\frac{S^2}{2} - S\left[\frac{1}{6} - \frac{A}{2} - B + \overline{U}\right])\times(1-S^3) \tag{62e}$$

$$\left.+\left(\frac{B}{2}\times(\frac{1}{6} - \frac{A}{2} - B + \overline{U}) + \frac{A}{2}\times(\frac{S^4}{24} - A\frac{S^3}{6} - B\frac{S^2}{2} - S\left[\frac{1}{6} - \frac{A}{2} - B + \overline{U}\right]\right)\times(1-S^2)\right\}.$$

Hence, the Nusselt number based on model A is [3]

$$Nu\big|_{\text{Model A}} = \frac{4\varepsilon k}{\Theta_w\big|_{\text{Model A}} - (I_A + II_A + III_A + IV_A)}. \tag{63}$$

The Nusselt number obtained based on model A, given by Eq. (63), is similar to that in Ref. [3].

2.5.2. Nusselt number for model B

Through the definition of Nusselt number in Eq. (57) and temperature solutions obtained in section 2.4.2, the Nusselt number based on model B can be derived. By setting Y=1 in Eq. (51a), model B gives the non-dimensional temperature of the fluid at the channel wall. This is

$$\Theta_w\big|_{\text{Model B}} = \varepsilon\psi\left(-\frac{1}{24}+\frac{A}{6}+\frac{B}{2}+O_1+O_2\right), \tag{64}$$

where O_1 and O_2 are given in Eqs. (51b) and (51c).

Similar to that presented for model A, the mean temperature Θ_m for model B can be stated as

$$\Theta_m\big|_{\text{Model B}} = I_B + II_B + III_B, \tag{65a}$$

where

$$\begin{aligned} I_B = {} & \frac{C\varphi 1}{2\Gamma^2}\left[\frac{\sinh(S(Z+\Gamma))}{Z+\Gamma}+\frac{\sinh(S(Z-\Gamma))}{Z-\Gamma}\right] \\ & +\left[\frac{C\varphi 2}{Z}-\frac{C^2\psi(Z^2-Bi)}{2Z^2(Z^2-\Gamma^2)}\cosh(ZS)+\frac{(Z^2S^2+2)CBiDa\psi}{2\Gamma^2Z^3}\right]\sinh(ZS) \\ & -\frac{CSBiDa\psi}{Z^2\Gamma^2}\cosh(ZS)-\frac{C^2S\psi(Z^2-Bi)}{2Z^2(Z^2-\Gamma^2)}, \end{aligned} \tag{65b}$$

$$II_B = \frac{Da\varphi 1}{\Gamma^3}\sinh(\Gamma S)+\frac{Da^2S^3Bi\psi}{6\Gamma^2}+S\varphi 2-\frac{DaC\psi(Z^2-Bi)}{Z^3(Z^2-\Gamma^2)}\sinh(ZS), \tag{65c}$$

and

$$\begin{aligned} III_B = {} & \varepsilon\psi\left\{\frac{1}{336}\times(1-S^7)+\frac{-A}{48}\times(1-S^6)+\left(-\frac{A^2}{30}-\frac{7B}{120}\right)\times(1-S^5)\right. \\ & +\left(-\frac{O_1}{8}+\frac{AB}{6}\right)\times(1-S^4)+\left(-\frac{O_2}{6}+\frac{AO_1}{3}+\frac{B^2}{6}\right)\times(1-S^3) \\ & \left.+\left(\frac{AO_2}{3}+\frac{BO_1}{2}\right)\times(1-S^2)+BO_2\times(1-S)\right\}. \end{aligned} \tag{65d}$$

Therefore, the Nusselt number based on model B is

$$Nu\big|_{\text{Model B}} = \frac{4\varepsilon k}{\Theta_w\big|_{\text{Model B}} - (I_B + II_B + III_B)}. \tag{66}$$

2.6. Pressure drop and heat transfer performance

The increase in the pressure drop is a serious drawback of heat transfer enhancement by porous media. A complete analysis should, therefore, consider both heat transfer rate and pressure drop. This analysis leads to obtain optimum value of porous thicknesses, which hold the maximum

Nusselt number with the expense of reasonable pressure drop. The pressure drop is related to the friction factor by [44]

$$f = (-\frac{\partial p}{\partial x})\frac{D_h}{1/2\rho\bar{u}^2}. \tag{67}$$

In the fully developed region, the pressure gradient is constant. Using the definition of the characteristic velocity u_r, the friction factor, f is obtained as [45]

$$f = \frac{8}{\bar{U}\,\mathrm{Re}}, \tag{68}$$

where Re is a macroscopic Reynolds number based on the fluid velocity and is defined as $\mathrm{Re} = \rho\bar{u}\mathrm{h}_0/\mu$. The effects of porous media on the heat transfer and pressure drop are collectively evaluated by the so-called Heat Transfer Performance (HTP) [45]. This has been defined as [45]

$$\mathrm{HTP} = \frac{(Nu)_p/(Nu)_o}{(f\,\mathrm{Re})_p/(f\,\mathrm{Re})_o}, \tag{69}$$

where indices "*p*" refers to a channel with porous material and "*o*" represents the channel without the porous material inserts. The value of HTP serves as a thermo-hydrodynamic measure of the heat transfer efficiency. Equation (69) shows that a clear channel corresponds to HTP value of one, which is the base case. Adding porous insert can result in increasing both heat transfer rate and pressure drop. The precise evaluation of HTP is important for design purposes [45]. To achieve this, the Nusselt numbers given by Eqs. (63) and (66) along with Eq. (28) can be readily substituted into Eq. (69) to develop an analytical expression for HTP.

3. Results and discussions

3.1. Validation

Figure 2 compares models A and B temperature distributions given by Eqs. (42, 43) and (52, 53) for a fully filled channel S=1, to those derived by Marafie and Vafai [30] and Yang and Vafai [25]. In the latter solution [25], the internal heat generations have been set to zero to become comparable to Eqs. (52, 53). An excellent agreement is observed between these solutions. The present solution also predicts the values of the Nusselt number for S=0.6, k=0.01, Bi=0.01 and Da=1 as Nu=8.249. This is very close to the value of Nusselt number in a channel without porous material, i.e. Nu=8.235 [42]. Furthermore, Eq. (63) predicts the Nusselt number for S=0.6, k=0.01, Bi=0.01 and Darcy number of Da=1, and Da=10 to be respectively 8.373 and 8.249. These are 1.77% and 0.19%, higher than the value of Nusselt number in a channel without porous material, i.e. Nu=8.235 [42]. The analytical solution, developed in section 2, is therefore capable of reproducing the existing results and shows a sensible physical behaviour.

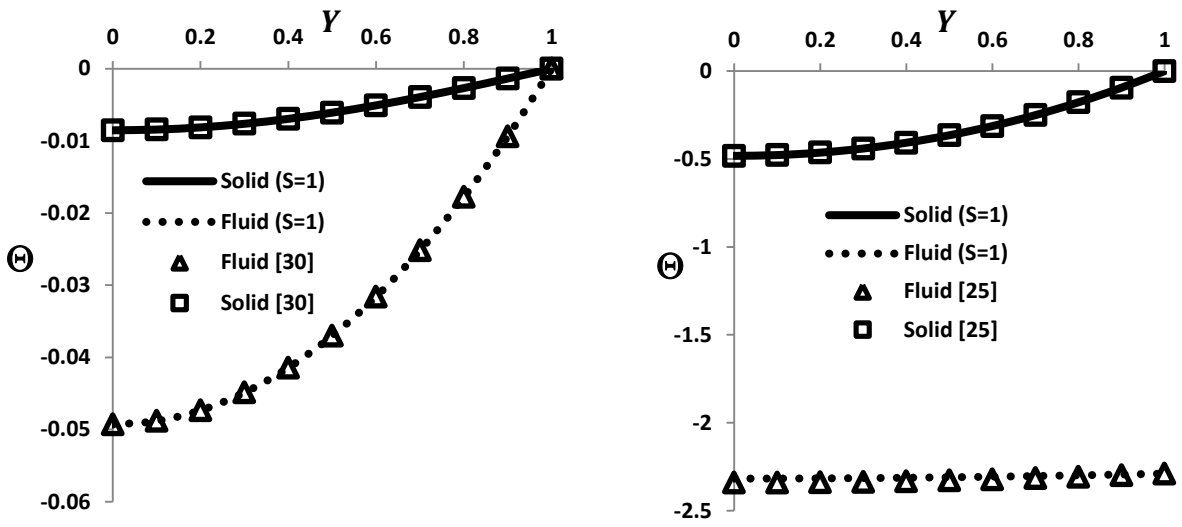

(a) (b)

Fig. 2. Temperature distributions for the fluid and solid phases at S=1, k=0.1, Bi=0.5 and Da=10^{-5}, continuous curves: the present solutions, dots: solutions in references [25, 30], (a) model A, Eqs. (42) and (43) and (b) model B, Eqs. (52) and (53).

3.2. Velocity distribution

Figures 3(a) and 3(b) illustrate the effect of porous substrate thickness on the axial velocity in the fully developed region for Da= 10^{-3} and 10^{-5} respectively. These figures show that by increasing the porous layer thickness the axial velocity in the clear region increases. This is because of the hydraulic resistance of the porous region against the flow. Hence, as the porous material thickness increases most of the fluid flows through the clear region. This intensifies the velocity gradient close to the interface of the fluid and porous medium. Further, as S increases the location of the maximum velocity in the clear region shifts towards the wall. After exceeding a certain porous medium thickness, the gap between the channel wall and the porous region becomes too small to handle the flow without a significant pressure drop. Thus, part of the flow is forced to move back into the porous region. The maximum velocity in the clear region, therefore, decreases in this case.

A comparison between Figs. 3a and 3b reveals that as Da number decreases the axial velocity in the porous substrate increases. This is due to the fact that at lower Da numbers the porous region is less permeable to the fluid flow and the fluid is forced to escape to the clear region. Therefore, the maximum velocity in the clear region increases. These figures, further, show that as Da number decreases the maximum velocity in the clear region moves towards the channel wall.

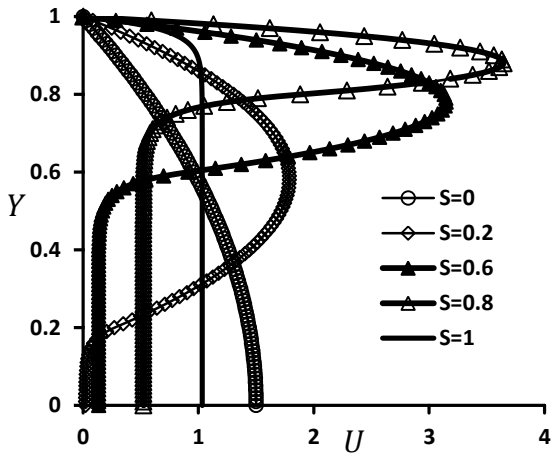

(a)

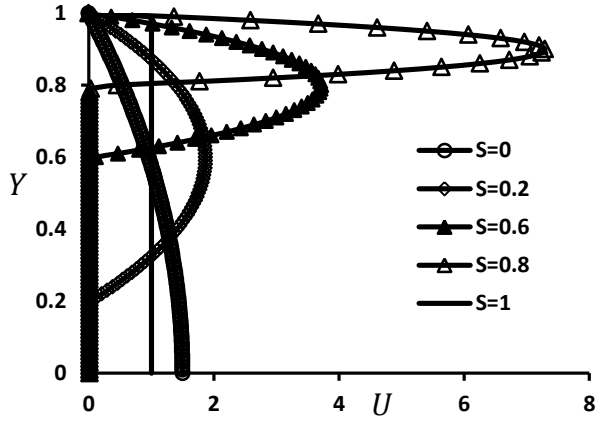

(b)

Fig. 3. Effect of porous substrate thickness on the axial velocity profile, (a) $Da=10^{-3}$ and (b) $Da=10^{-5}$.

3.3. Heat flux distribution at the porous-fluid interface

Equations (30) and (32) indicate that the interface heat flux is, in general, a function of porous medium thickness, Darcy number and the interface model. Figure 4 shows the ratio of the interface heat flux to that of the wall (see Eq. (22c)) for models A and B. It is clear that through changing the interface model, the distribution of heat flux ratio versus porous medium thickness remains qualitatively unchanged. However, the value of heat flux transferred to the porous region depends on the specific model used at the porous-fluid interface. Clearly, almost at any given S and Da, model B predicts a smaller heat flux ratio. As Da decreases, the difference between the thermal fluxes predicted by the two models becomes smaller. A range of Da values was considered and it was found that the two values of Da shown here are enough to represent the influence of this parameter.

For a given model increasing the porous thickness increases the amount of heat flux transferred to the porous region. This is due to the increase in the maximum flow velocity in the clear region and the velocity gradient near the wall and the interface at higher S values (see Fig. 3). Hence, through Reynolds analogy [46] an increase in the amount of heat flux at the interface is expected. Furthermore, for a fixed model reduction of Da number results in a smaller flow entering the porous region and consequently reduces the amount of heat flux at the porous-fluid interface.

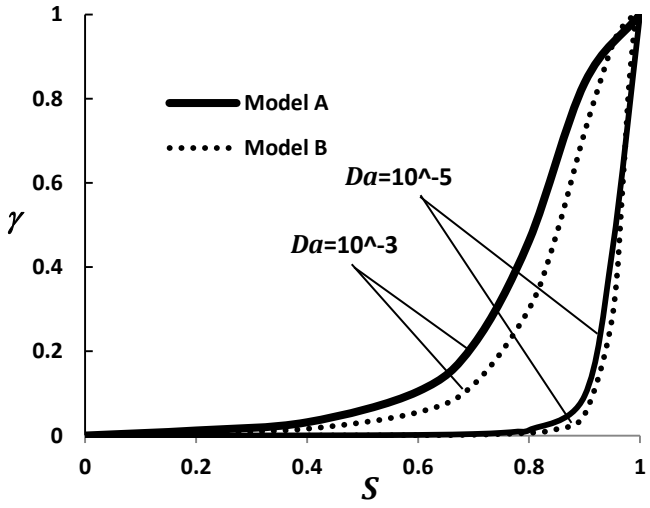

Fig. 4. Effect of porous medium thickness on the heat flux distribution.

3.4. Temperature distributions by models A and B and validity of LTE

Figures 5 and 6 show the dimensionless temperature distributions for model A (Eqs. (42) and (43)) and model B (Eqs. (52) and (53)) at S=0.9 and different values of Bi, k and Da. Considering model A the effects of Bi, k, Da and S on the validity of LTE has been discussed elsewhere [3]. Here, the main purpose is to compare the influences of different interface models upon the validity of LTE. Local thermal equilibrium holds when the maximum of absolute temperature difference between the solid and fluid phases within the porous region is very small, i.e. $\max|\Theta_s - \Theta_f| \cong 0$. For a high Darcy number (Da=10^{-3}), Fig. 5a shows that at low k and low Bi, model A results in a negligible temperature difference between the two phases and hence LTE remains valid. However, the temperature difference between the two phases is large under model B and therefore in this case LTNE holds. Further, in the interface region and under model B the temperature difference between the two phases is smaller compared to that at the core of the porous medium. A comparison between Figs. 5b and 5a reveals that for low k, as Bi increases (see Fig. 5b) the non-dimensional fluid and solid temperatures decrease. Hence, the temperature difference between the two phases

decreases. This is because of the significant heat transfer between the fluid and solid matrix at high *Bi* number, which reduces the temperature difference between the two phases. Figure 5b further shows that unlike model A, model B results in a considerable temperature difference between the two phases in the whole porous region and therefore this model predicts LTNE condition. For high *k* and low *Bi,* however, both models predict LTNE condition, see Fig. 5c. Once again, the temperature difference between the two phases predicted by model B is larger than that of model A. Figures 5a shows that under model B and for fixed *Bi* as *k* increases the temperature difference between the solid and fluid phases, decreases. The same trend can be observed in Fig. 5c for model B. Further, as *k* increases, the temperature difference between the two phases along the *Y* axis decreases and the maximum temperature difference occurs at *Y*=0.9. This indicates that the effect of *k* on reducing the temperature difference is more significant in the regions close to the interface.

Figure 5d corresponds to high values of *k* and *Bi*. It is clear from this figure that at this limit the predictions of the two models are close to each other. Figure 5d further shows that both models predict considerable temperature differences between the two phases. Therefore, regardless of the interface model LTNE holds in this figure.

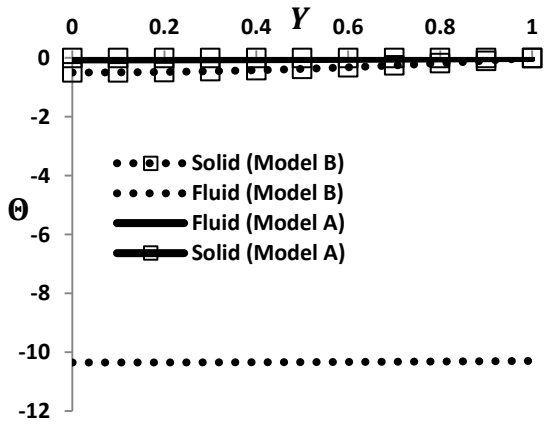

(a) *k*=0.1, *Bi*=0.1

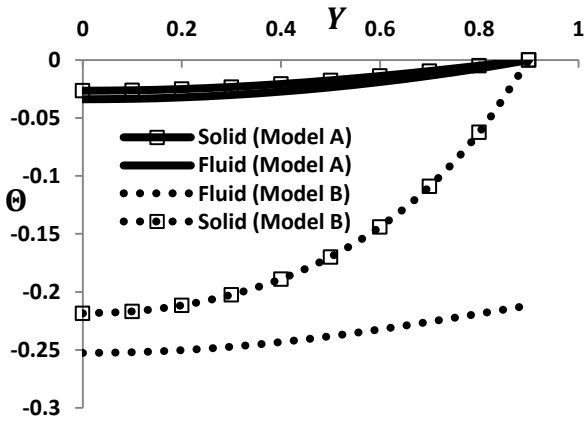

(b) *k*=0.1, *Bi*=10

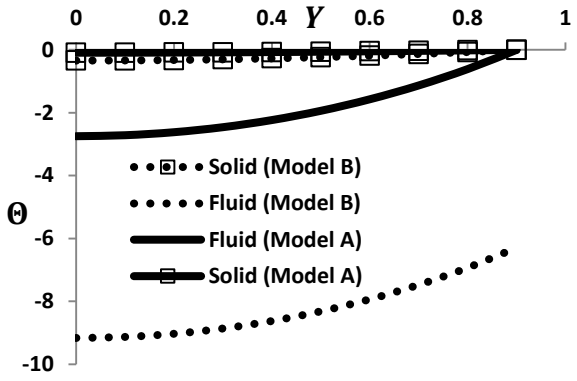

(c) k=10, Bi=0.1

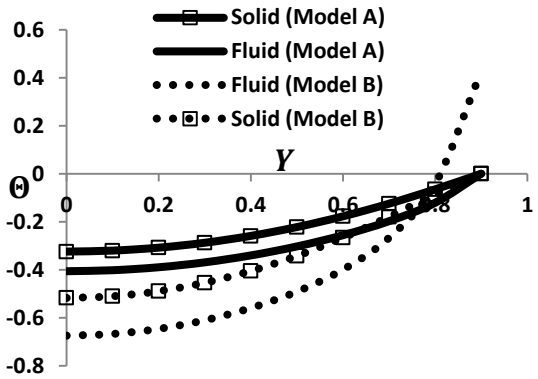

(d) k=10, Bi=10

Fig. 5. Temperature distributions for fluid and solid phases, S=0.9, Da=10^{-3}.

Figure 6 depicts the same type of information as Fig. 5 for a lower value of Da (Da=10^{-5}). It is noted that the general trend of temperature distribution, in here, is similar to that observed in Fig. 5 for Da=10^{-3}. Nonetheless, smaller values of Da have resulted in the reduction of the dimensionless temperatures. The temperature difference between the two phases also decreases. Hence, it may be concluded that as Da decreases LTE condition is approached. Further discussion on the validity of LTE under model A and for varying Bi, k and Da can be found in Ref. [3].

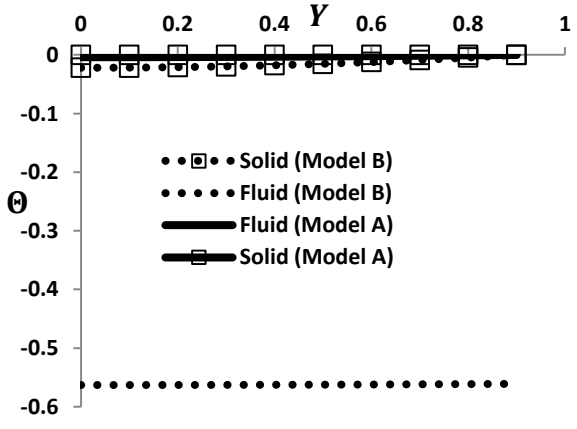

(a) k=0.1, Bi=0.1

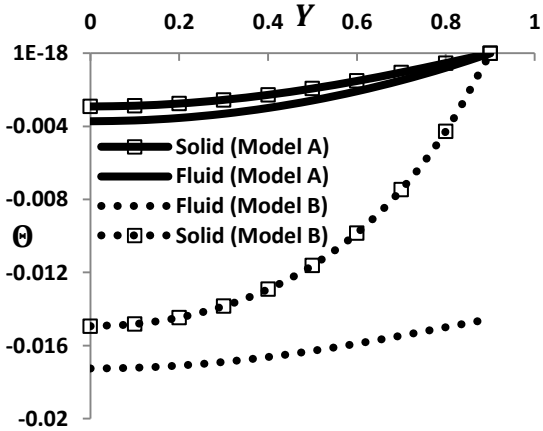

(b) k=0.1, Bi=10

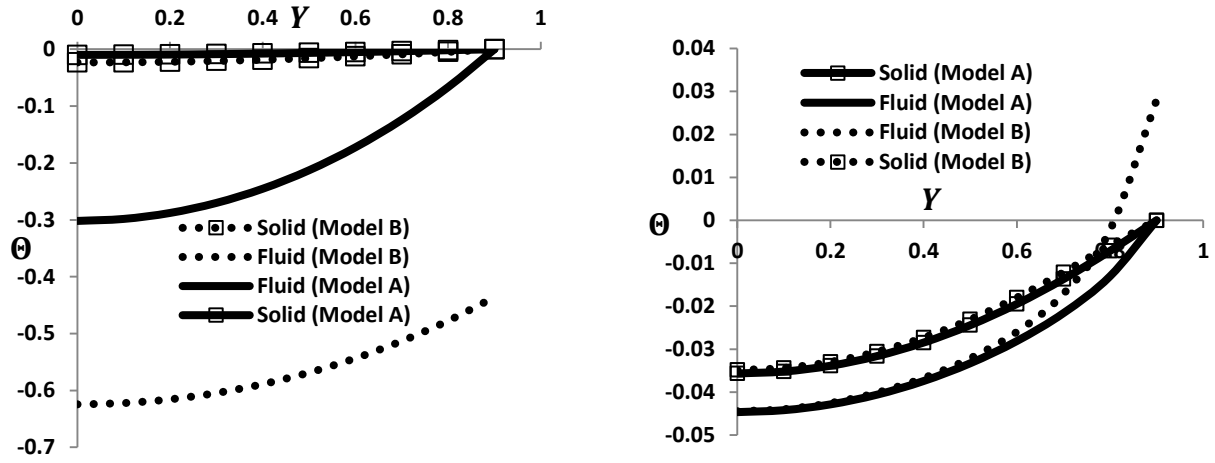

(c) k=10, Bi=0.1 (d) k=10, Bi=10

Fig. 6. Temperature distributions for fluid and solid phases, S=0.9, Da=10^{-5}.

3.5. Critical values of porous thickness for validity of LTE

In general, a number of factors can affect the validity of LTE. These include the ratio of porous material thickness to channel height, the porous-fluid interface model, Darcy number, k and Biot number. To evaluate the relative significance of these factors, this section examines the maximum temperature difference between the two phases under varying parameters. This is defined as $\max|\Theta_s - \Theta_f|$ and Fig. 7 presents the corresponding results for different values of k and Bi. This figure shows that as the porous medium thickness (S) increases the maximum temperature difference between the two phases increases. In all investigated cases the maximum temperature difference is reached at S=1. It is inferred from Figs. 7a-d that for all considered values of k, Bi and Da as S exceeds 0.9 the LTE assumption becomes invalid. Importantly, for low Da numbers (Da<10^{-3}) and at S=1 the two models A and B result in the same temperature difference between the two phases. Hence, for Da<10^{-3} and S~1 the temperature difference is deemed independent of the interface model. Figure 7a shows that for a fixed Da, high k and low Bi, increase of the porous material thickness signifies the difference between the outcomes of the two models. Further, for a fixed porous material thickness as Da increases the difference between the predicted temperatures by the two models appreciates. Nonetheless, there exists a maximum value of the porous medium thickness up to that the difference between the predictions of the two models is negligible. This value is of significance because it draws a boundary below which the two models are acting similarly. It is, therefore, regarded as a critical value, $S_{\mathrm{ctr},\Delta\Theta}$. In Fig. 7a as Da decreases from 10^{-3} to 10^{-5} , $S_{\mathrm{crt},\Delta\Theta}$ varies from 0.1 to 0.9.

Another critical thickness, $S_{ctr,LTE}$, is further defined as the maximum porous thickness for which each model predicts LTE. As stated earlier, validation of the LTE assumption leads to major simplifications, since it eliminates the need for solving two energy equations. It follows that detection of the maximum porous insert thickness, which allows the LTE assumption, is an important issue. Figure 7a shows that for the higher value of *Da* ($Da=10^{-3}$) the critical LTE porous thickness, $S_{ctr,LTE}$, is strongly model dependent. For instance, model B predicts the critical thickness as $S_{ctr,LTE}$ =0.2. However, considering model A this value increases to $S_{ctr,LTE}$ =0.6. This behaviour changes at low *Da*, such that for both interface models the critical porous medium thickness is 0.9.

At high values of *k* and *Bi,* as shown in Fig. 7b, the two models feature similar results for a wider range of the thickness ratio. In this figure, the critical thicknesses in which the two models show similar results correspond to $S_{ctr,\Delta\Theta}$ =0.7 and $S_{ctr,\Delta\Theta}$ =0.9 for $Da=10^{-3}$ and $Da=10^{-5}$. A comparison between Figs. 7a and 7b reveals that at low *Da* number the critical thickness for LTE validity, $S_{ctr,LTE}$, is independent of the interface model and *Bi* number. Figure 7c corresponds to low values of *k* and *Bi*. In this figure, for both values of *Da* number and under model A, LTE is valid for the entire range of *S*, i.e. $S_{ctr,LTE}$ =1. Considering model B in this figure, for $Da=10^{-3}$, the critical porous medium thickness is $S_{ctr,LTE}$ =0.2 and as *Da* decreases to 10^{-5} the critical thickness increases to $S_{ctr,LTE}$ ~1. In Fig. 7d the value of *k* is low while *Bi* is high. The general trend of temperature difference is similar to Fig. 7b but here the numerical values of the temperature difference are an order of magnitude smaller.

It is concluded from the preceding discussion that for all values of *k*, *Bi* and *Da* and for the porous thickness higher than 0.9, the LTE assumption is invalid under either of the two interface models. Further, for the fully filled channel and high Darcy number the maximum temperature difference between the two phases depends on the interface model. For instance, in Fig. 7d for $Da=10^{-3}$ and *S*=1, model A predicts $\Delta\Theta_{max} \cong 0.01$. However, under model B this changes to $\Delta\Theta_{max} \cong 0.25$.

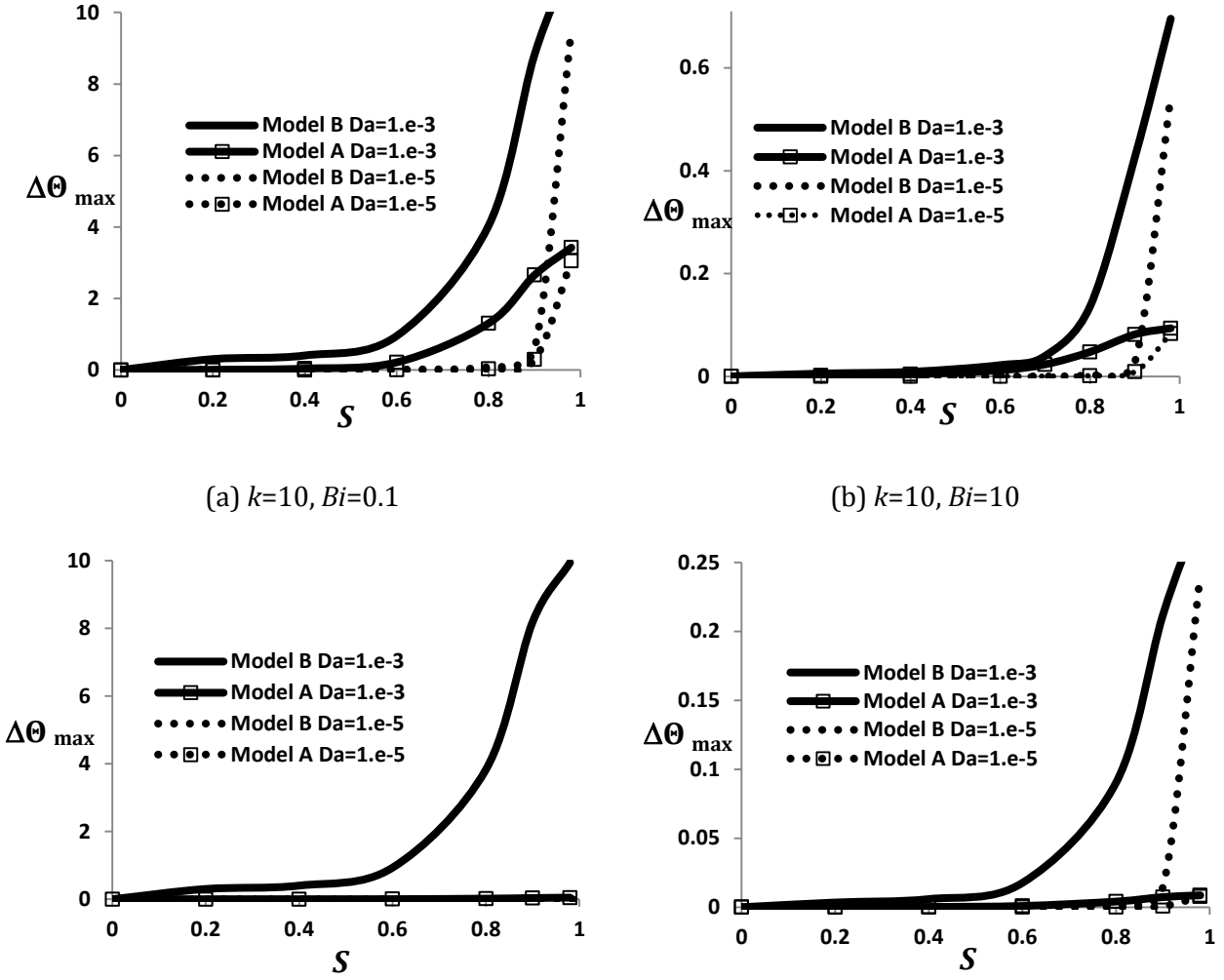

(a) k=10, Bi=0.1

(b) k=10, Bi=10

(c) k=0.1, Bi=0.1

(d) k=0.1, Bi=10

Fig. 7. Maximum temperature difference between the solid and fluid phase within the porous region.

1

2 **3.6. Nusselt Number**

3 It was shown in section 2.5 that fully developed Nusselt number is a function of porous substrate
4 thickness, *Da*, *Bi*, *k* and the two interface models A and B. Figure 8 shows the variation of Nusselt
5 number in the porous region predicted by Eqs. (63) and (66) for models A and B. Figure 8a
6 illustrates the results obtained for k=10 and Bi=10, and a wide range of *Da* number. In this case the
7 trend of variation of *Nu* number versus *S* for $Da=10^{-3}$ is different to those at other *Da* numbers. For
8 model B and $Da=10^{-3}$, the variations of the *Nu* as a function of *S* can be divided into three stages.
9 During the first stage, the *Nu* number increases with *S* up to about *S*=0.8. For larger values of *S*, the
10 second stage, as *S* increases the *Nu* number decreases. The third stage includes values of *S* close to 1

for which Nusselt number again increases with S. At smaller Darcy numbers in model B, Nusselt number graphs in Fig. 8a feature only two stages. First, Nu number monotonically increases with S. After reaching a local maximum, further increase in S results in the reduction of the Nu number. There are, therefore, extremum values of S, which correspond to the maximum of Nusselt number for each value of Darcy number. We refer to these extremum points as the optimum Nusselt thicknesses of the porous medium ($S_{opt,Nu}$). The values of this quantity for model B are 0.85, 0.9 and 0.95 at Da numbers of 10^{-4}, 10^{-5} and 10^{-6}, respectively.

For model A and all considered Da numbers, Fig. 8a shows that Nusselt number monotonically increases with porous medium thickness over the entire range of S. Thus, the fully filled channel (S=1) yields the highest value of Nu number. It can be seen in Fig. 8a that at fixed Da and for S larger than a specific value, the Nu number based on model A is higher than that based on model B. This is to be expected since model A leads to a larger enhancement of heat transfer compared to model B [19]. Further, according to Fig. 4 under model A more heat flux is transferred to the porous region. Therefore, a larger fraction of the heat flux at the interface, $q_{interface}$, is transferred to the porous region. It follows that the Nusselt number calculated from model A is higher than that obtained through model B [19]. Furthermore, in Fig. 8a for a fixed model, as Da number decreases, Nu number increases. The effects of S and Da on Nu number can be explained using the velocity distribution shown in Fig. 3. It is clear from this figure that as Da decreases and/or S increases the maximum velocity in the clear region increases. Hence, by Reynolds analogy the heat transfer rate and the Nu number are expected to increase [3, 5, 19].

It is observed in Figs. 8a-d that for each Da number there is a critical porous thickness below which the Nu numbers obtained by the two models are almost the same ($S_{crt,Nu}$). In Fig. 8a for instance, for Da numbers of 10^{-3}, 10^{-4}, 10^{-5} and 10^{-6} the values of $S_{crt,Nu}$ are 0.8, 0.8, 0.85 and 0.9, respectively. Clearly, reduction of Da widens the range of the porous medium thickness at which the two models predict similar Nu number.

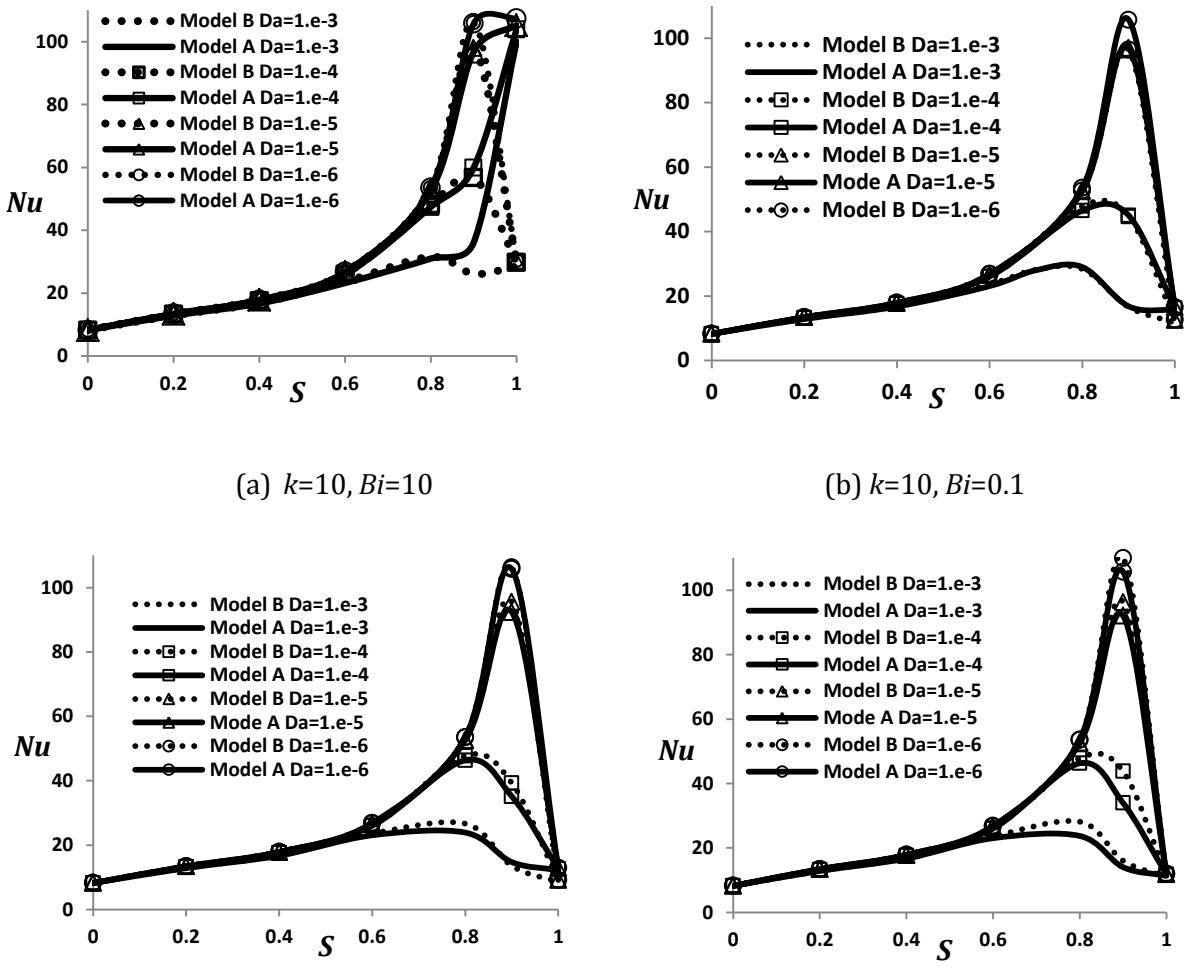

(a) k=10, Bi=10 (b) k=10, Bi=0.1

(c) k=0.1, Bi=10 (d) k=0.1, Bi=0.1

Fig. 8. Nusselt number versus the ratio of porous medium thickness to channel height (S).

More qualitative agreements are observed between the two interface models in Fig. 8b, which corresponds to k=10 and Bi=0.1. In this figure, the total S range can be divided into two regions. In the first region, Nu increases monotonically with S and reaches a maximum. The increase of Nusselt number, in this region, significantly intensifies for S>0.6. Conversely, Nusselt number decreases sharply in the second range, which includes the values of S close to unity. In Fig. 8b for both interface models the values of $S_{opt,Nu}$ which maximise the Nu number are 0.7, 0.8, 0.9 and 0.95 for Darcy numbers of 10^{-3}, 10^{-4}, 10^{-5} and 10^{-6}, respectively. Further, Figs. 8a and 8b show that for Da numbers of 10^{-3}, 10^{-4}, 10^{-5} and 10^{-6} the values of $S_{crt,Nu}$ are respectively 0.6, 0.8, 0.9 and 0.9. In Fig. 8b as Da number decreases, for all values of S with the exception of S=1, the two models predict very

similar *Nu* numbers. This, once again, shows that for low *Da* numbers the results of the two models A and B approach each other.

In Fig. 8c the values of k and Bi are respectively 0.1 and 10. It is clear in this figure that for values of S less than 1, the two models result in very similar *Nu* numbers. However, close inspection of Fig. 8c reveals that at S=1 the *Nu* numbers obtained by the two models are slightly different, in which model A leads to higher *Nu* numbers. For both models and for Darcy number of 10^{-3}, 10^{-4}, 10^{-5} and 10^{-6} the values of $S_{\mathrm{opt,Nu}}$ are respectively 0.8, 0.8, 0.9 and 0.9.

Nusselt number variation with porous medium thickness and interface model for k=0.1 and Bi=0.1 has been shown in Fig. 8d. The qualitative behaviour in this figure is quite similar to that in Fig. 8c. However, for those values of S higher than the critical values ($S_{\mathrm{crt,Nu}}$), as S increases the difference between the two models A and B increases. The critical porous medium thicknesses ($S_{\mathrm{crt,Nu}}$) in which the two models predict similar results are 0.6, 0.8, 0.9 and 0.9 for *Da* numbers 10^{-3}, 10^{-4}, 10^{-5} and 10^{-6}, respectively.

The foregoing discussion implies that for each *Da* number there is a threshold of porous medium thickness below which *Nu* number is independent of Bi, k and even the interface model. These threshold values are respectively 0.6, 0.8, 0.8, 0.9, for *Da* number of 10^{-3}, 10^{-4}, 10^{-5} and 10^{-6}. It is further noted that for S=1 the *Nu* number is independent of *Da* and is just a function of the interface model. This is a consequence of using a Darcian flow model in the present analysis. Furthermore, at S=1 the *Nu* number obtained by model A is always higher than that of model B.

3.7. Pressure drop and heat transfer performance

Figure 9 shows the variation of the pressure drop for the fully developed flow, represented by fRe in Eq. (68), versus porous medium thickness ratio. For a constant *Da* number the pressure drop increases almost monotonically with S. Further, at any value of S the pressure drop increases as *Da* decrease. This becomes more noticeable at larger values of S. Clearly, the pressure drop for the fully filled channel configuration is much higher than that in the partially filled duct. It is further noted that, for $Da<10^{-3}$ and S less than 0.8 the effect of Darcy number on the pressure drop is insignificant. Further, it was discussed in the previous section that for S=0.8 the obtained *Nu* number is much larger than that of the clear channel. Thus, S= 0.8 can be considered as the optimum thickness of the porous material for enhancing heat transfer.

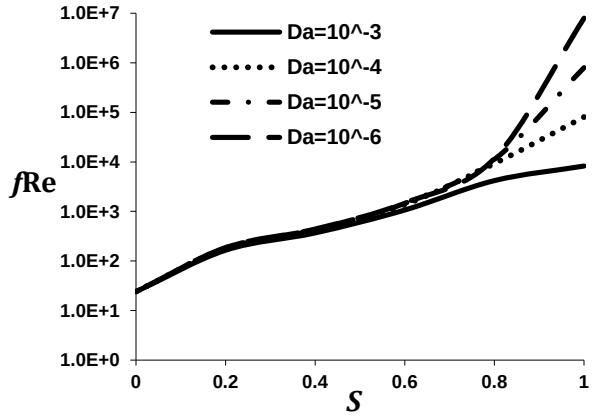

Fig. 9. Non-dimensional, fully developed pressure drop versus non-dimensional porous substrate thickness at different Darcy numbers.

Heat transfer performance (HTP) was defined in Eq. (69) as the normalised ratio of Nusselt number and pressure drop. Figure 10 presents the variation of HTP, on the logarithmic scale, with S, k, Bi, and the two porous-fluid interface models. The value of HTP at S=0, representing a clear channel, is equal to 1. Through increasing the porous substrate thickness, HTP decreases owing to the significantly higher pressure drops compared to that in the clear channel.

Figure 10a shows that for high values of k, Bi and Da (Da=10^{-3}) and under model A, the variation of HTP versus S includes two stages. In the first stage as S increases up to 0.9, HTP decreases monotonically. Further increase in S causes an increase in HTP. However, under model B variation of HTP with S is simple and features a monotonic decrease over the entire range of S. This behaviour is repeated at all considered cases with Da<10^{-3} regardless of the employed interface model. It is clear in Fig. 10 that up to S=0.7, HTP remains independent of Da and the interface model. The influences of these factors become only noticeable at higher values of S. Figure 10a further shows that for Da<10^{-3} and S<0.9, HTP is independent of Da and the interface model. However, for S>0.9 HTP strongly depends on Da and the model used at the interface. In this limit, for a fixed model, reduction of Da results in lower HTP values. Further, for any fixed Da number, model B predicts a lower value of HTP compared to that obtained by model A.

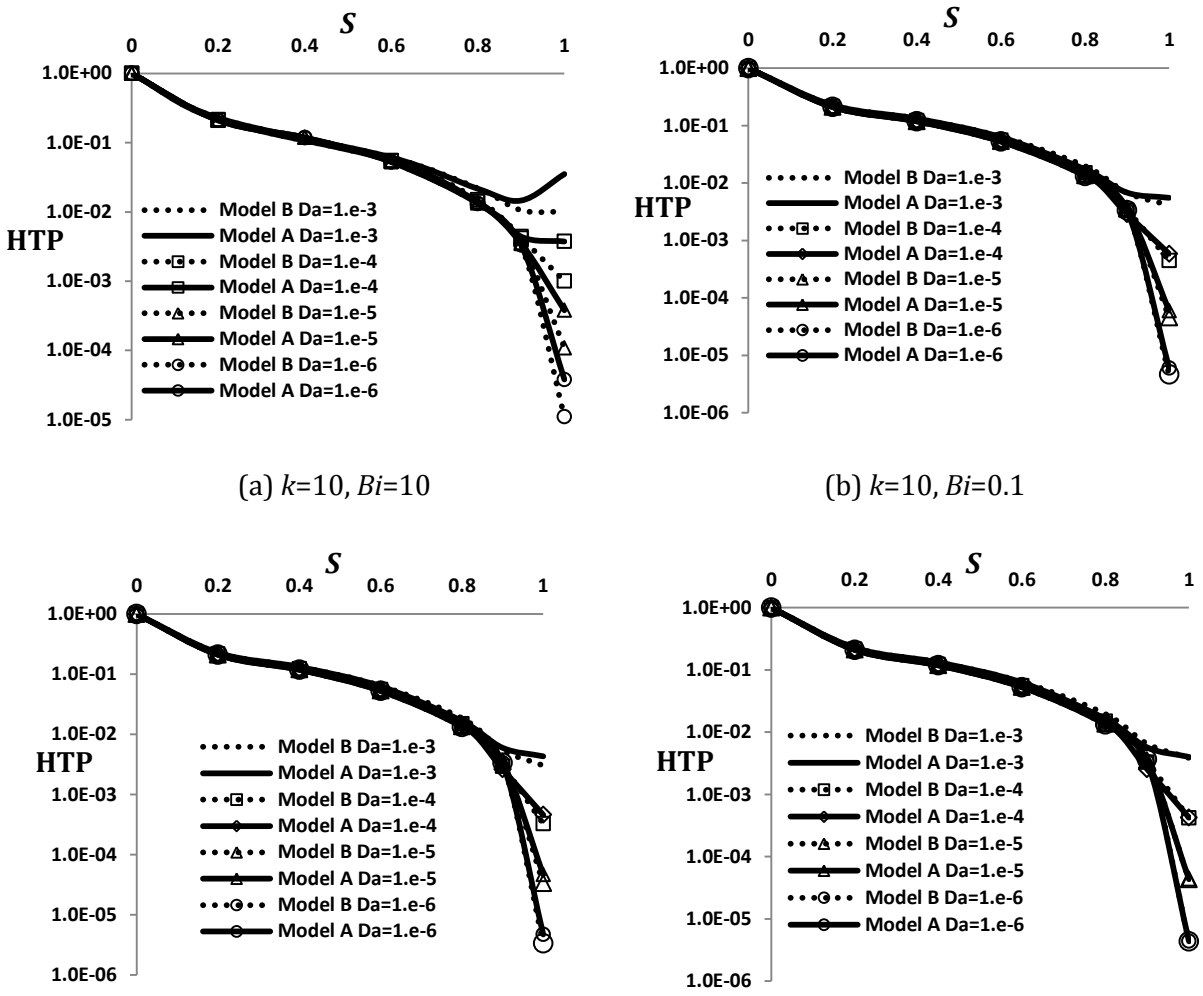

(a) k=10, Bi=10 (b) k=10, Bi=0.1

(c) k=0.1, Bi=10 (d) k=0.1, Bi=0.1

Fig. 10. Heat transfer performance (HTP) versus the porous medium thickness ratio.

Decreasing Bi to 0.1 in Fig. 10b simplifies the behaviour of HTP. In this case, for all considered Da numbers both models A and B predict the same trend of variation of HTP against S. Further, for all Da numbers and S<0.9 the values of HTP are similar and independent of Da number. A slight difference is observed between the HTP obtained by the two models at S close to 1 in which model B predicts a lower HTP. By decreasing k in Fig 10c (k=0.1, Bi=10) the qualitative trend and the value of HTP remain almost unchanged. However, the difference between the two models in predicting HTP at S=1 is larger in this case. Furthermore, it is observed that for S<0.9 the variation of HTP versus S is independent of the Da number and the model used at the interface. Figure 10d presents low values of k and Bi numbers. Once again, the qualitative behaviour of HTP as a function of S is similar to those shown in Figs. 10b and 10c. In this case, both models predict very similar values of

HTP at different *Da* numbers. Here again, for $S<0.9$ the variation of HTP with *S* is independent of the *Da* number and the interface model.

It is evident from Fig. 10 that HTP for all pertinent parameters is lower than that of a clear channel. It should be noted, however, that introducing porous insert can lead to significant increase of the Nusselt number (see Fig. 8). Yet, the induced pressure drop, although smaller than that in the full porous case, is still substantial. Therefore, it drives the HTP towards the values less than one. In this sense, HTP can be seen as an unavoidable price of enhancing the heat transfer rate using porous media. Nonetheless, there are several applications where pressure drop is not a serious concern, as in the case of automobile or offshore drilling applications [47]. In these cases, porous materials can be used to increase the rate of heat transfer regardless of the induced pressure drop. The observed trend of HTP is in agreement with the experimental observations of Kang-Hoon Ko and Anand [47] who studied heat transfer enhancement in a rectangular channel with porous baffles. These authors reported that the ratio of heat transfer increase to unit increase in pumping power (the pumping power was proportional to the one-third power of the friction factor) was less than one [47]. Recently, Cekmer et al. [45] used the heat transfer and pressure drop increment ratio to define an overall performance of an inserted porous layer in a parallel plate channel under LTE. In their study for all operating conditions, the HTP was found to be less than unity [45].

4. Conclusions

In this study, forced convection of heat in a channel partially filled with a porous material was investigated analytically. Energy equations for both solid and fluid phases in the porous medium were solved assuming local thermal non-equilibrium (LTNE) condition and using Darcy-Brinkman model. Two existing models were used to describe the thermal boundary condition at the porous medium-fluid interface. In keeping with the literature, these were referred to as models A and B. Model A assumes that the heat division between the two phases is based on the physical values of their effective conductivities and their corresponding temperature gradients. In model B, however, each phase at the interface receives an equal amount of heat flux. Exact solutions were developed for the Nusselt number and temperature distributions in the fluid and solid phases. These solutions were obtained for each of the interface models and are, in general, functions of porous material thickness (*S*), Biot number (*Bi*), thermal conductivity ratio (*k*) and Darcy number (*Da*). A comparative parametric study was then conducted. The disparities between the two models in predicting the local thermal equilibrium (LTE) was further discussed. The Nusselt number and pressure drop ratio were finally combined to determine the heat transfer performance.

The major remarks on the behaviour of the investigated system can be summarised as follows.

- For high *Da*, low *k* and high *Bi*, application of model A results in a small temperature difference between the two phases and hence LTE becomes valid. However, using model B leads to large temperature differences between the two phases and implies LTNE.
- For high *k* and high *Bi,* both models predict LTE condition. Further, the temperature difference between the two phases obtained by model B is larger than that obtained by model A.
- For high *k* and high *Bi,* the results of the two models approach each other and indicate LTNE.
- As *Da* decreases the temperatures of the solid and fluid phases decrease and hence LTE is approached.
- For all considered values of *k* and *Bi* the *Nu* number using model A is higher than that obtained by model B.
- For all values of *k* and *Bi* and for each considered value of *Da*, there is a critical porous medium thickness below which the *Nu* numbers obtained by the two models are almost the same. For example, at high *k* and *Bi*, *Da* numbers of 10^{-3}, 10^{-4}, 10^{-5} and 10^{-6} correspond to the critical thickness ($S_{crt,Nu}$) values of 0.8, 0.8, 0.85 and 0.9.
- For low *Da* numbers, the two models result in similar *Nu* numbers for a wide range of porous medium thickness.
- For almost all values of *k* and *Bi* (except for high *k* and *Bi*) the variation of *Nu* number versus *S* includes two stages. In the first stage Nusselt number increases with *S* and there exists an optimum *S* that maximises the *Nu* number. In the second stage as *S* further increases, the *Nu* number decreases. For instance, at high *k*, low *Bi* and under both interface models the maximum *Nu* number is reached at *S* values of 0.7, 0.8, 0.9 and 0.95 for Darcy numbers of 10^{-3}, 10^{-4}, 10^{-5} and 10^{-6}, respectively.
- For high *k* and *Bi*, model B and $Da=10^{-3}$, the variations of Nusselt number as a function of *S* is divided into three stages. During the first stage, the *Nu* number increases as *S* increases up to $S=0.8$. The second stage includes values of *S* more than 0.8 in which as *S* increases the *Nu* number decreases. Further increase of *S*, in the third stage, causes the porous-fluid interface to reach the channel wall and the *Nu* number increases. For $Da<10^{-3}$ and under model B the variation of *Nu* number is divided into two stages. Finally, under model A and for all *Da* numbers the variation of *Nu* number versus *S* is single stage. This features a

monotonic increase of the *Nu* number with *S.* Thus, the fully filled channel has the highest *Nu* number.

- For all values of *k* and *Bi*, at *S*=1, *Nu* number is independent of *Da* and is just a function of the interface model used at the porous -fluid interface.
- By increasing *S* the value of HTP decreases and becomes less than unity, which corresponds to a clear channel.
- In general, at all values of *k* and *Bi*, and for *S*<0.9 the variation of HTP with *S* is independent of *Da* number and the model used at the porous-fluid interface.

The most distinctive feature of this work was the inclusion of LTNE condition through an analytical approach. This paper supplements and significantly advances the earlier study of Mahmoudi and Marefat [3]. In particular, implementation of the LTNE in a partial porous configuration through model B, comparison with model A and all the related discussions were completely novel. The results showed that applying different boundary conditions at the interface of the porous and clear regions could lead to considerably different Nusselt numbers and heat transfer performances. This highlights the necessity of further research on the characterisation of porous-fluid interface.

Nomenclature

a_{sf}	Interfacial area per unit volume of porous media (m^{-1})
A	Constant parameter defined by Eq. (24)
B	Constant parameter defined by Eq. (25)
Bi	Biot number, $\frac{a_{sf} h_{sf} h_0^2}{(1-\varepsilon)k_s}$
C	Constant parameter defined by Eq. (27)
C_p	Specific heat of the fluid, (J $Kg^{-1}K^{-1}$)
Da	Darcy number, K/h_o^2
D_h	Hydraulic diameter of the channel ($4h_0$)
f	Friction factor
h_{sf}	Fluid to solid heat transfer coefficient (W $m^{-2}K^{-1}$)
h_0	Height of the channel (m)
h_p	Porous substrate thickness (m)
K	Permeability of the porous medium (m^2)

k	The ratio of solid effective thermal conductivity to that of the fluid, $(1-\varepsilon)k_s/(\varepsilon k_f)$
k_f	Thermal conductivity of the fluid (W $m^{-1}K^{-1}$)
$k_{f,eff}$	Effective thermal conductivity of the fluid, εk_f
k_s	Thermal conductivity of the solid (W $m^{-1}K^{-1}$)
$k_{s,eff}$	Effective thermal conductivity of the solid, $(1-\varepsilon)k_s$
Nu	Nusselt number
O_1	Constant parameter defined by Eq. (51b)
O_2	Constant parameter defined by Eq. (51c)
p	Pressure (Pa)
q	Heat flux (W m^{-2})
Re	Reynolds number, $\mathrm{Re} = \rho \bar{u} \mathrm{h}_0 / \mu$
S	Ratio of the porous medium thickness to the channel height, h_p/h_0
$S_{crt,\Delta\Theta}$	Critical S up to which the two models A and B show similar results of the maximum temperature difference between two phases
$S_{crt,LTE}$	Critical value of S up to which the LTE condition validates
$S_{opt,Nu}$	Optimum value of S which maximises the Nusselt number
$S_{crt,Nu}$	Critical value of S up to which both models predict the same Nu number
T	Temperature (K)
T_m	Average temperature (K)
u	Longitudinal velocity (m/s)
$\bar{u}$	Average velocity
u_r	Characteristic velocity, $-\frac{h_0^{\,2}}{\mu}\frac{\partial p}{\partial x}$
U	Dimensionless velocity, u/u_r
$\bar{U}$	Dimensionless average velocity
x	longitudinal coordinate (m)
y	Transverse coordinate (m)
Y	Dimensionless y coordinate, y/h_0
Z	Constant parameter, $\sqrt{1/Da}$
Greek symbols	
γ	Ratio of wall heat flux to the heat flux at the interface, $q_w/q_{interface}$
Γ	Constant parameter defined by Eq. (54e)
ε	Porosity of the porous medium
Θ	Dimensionless temperature

μ	Viscosity (kg $m^{-1}s^{1}$)
ρ	Density, (kg/m^3)
ξ	Constant parameter used in Eq. (43)
ψ	Constant parameter defined by Eq. (54e)
$\varphi 1$	Constant parameter defined by Eq. (54b)
$\varphi 2$	Constant parameter defined by Eq. (54c)
$\varphi 3$	Constant parameter defined by Eq. (54d)
Subscripts	
eff	Effective property
exchange	internal heat exchange
f	Fluid
f1	Fluid in the clear region
f2	Fluid in the porous medium
in	Inlet
m	mean
o	Open channel without porous material
p	Porous medium
s	Solid
w	Wall
interface	The interface between the porous medium and the clear region
Superscripts	
–	Mean value
$','',''',''''$	First, second, third, and forth derivatives with respect to Y

1

2 **References**

3

[1] S. Kakac, A.E. Bergles, F. Mayinger, H. Yuncu (eds), Heat Transfer Enhancement of Heat Exchangers, Proceedings of the NATO Advanced Study Institute, held in Çesme-Izmir, Turkey, 1999, Kluwer Academic, Dordrecht, The Netherlands, 1999.

[2] K. Vafai, Handbook of Porous Media, Marcel Dekker, Ohio, 2000.

[3] Y. Mahmoudi, M. Maerefat, Analytical investigation of heat transfer enhancement in a channel partially filled with a porous material under local thermal non-equilibrium condition, Int. J. Thermal Sciences 50 (2011) 2386-2401.

[4] A.A. Mohamad, Heat transfer enhancement in heat exchangers fitted with porous media, Part I: constant wall temperature, Int. J. Thermal Sciences 42 (2003)385-395.

[5] M. Maerefat, S.Y. Mahmoudi , K. Mazaheri, Numerical simulation of forced convection enhancement in a pipe by porous inserts, Heat Transfer Engineering 32 (2011) 45-61.

[6] D. Poulikakos, M. Kazmierczak, Forced convection in a channel filled with porous medium, including the effect of flow inertia, variable porosity, and Brinkman friction, ASME J. Heat Transfer 109 (1987) 880-888.

[7] M.A. Al-Nimr, M.K. Alkam, Unsteady non-Darcian forced convection analysis in an annulus partially filled with a porous material, ASME J. Heat Transfer 119 (1997) 799-804.

[8] M.K. Alkam, M.A. Al-Nimr, M.O. Hamdan, Enhancing heat transfer in parallel-plate channels by using porous inserts, Int. J. Heat Mass Transfer 44 (2001) 931-938.

[9] B.I. Pavel, A.A. Mohammad, An experimental and numerical study on heat transfer enhancement for gas heat exchangers fitted with porous media, Int. J. Heat and Mass Transfer 47 (2004) 4939-4952.

[10] V.V. Satyamurty, D. Bhargavi, Forced convection in thermally developing region of a channel partially filled with a porous material and optimal porous fraction, Int. J. Thermal Sciences 49 (2010) 319-332.

[11] K. Vafai, S.J. Kim, Analysis of surface enhancement by a porous substrate, Trans. ASME. J. Heat Transfer 112 (1990) 700–706.

[12] H. Shokouhmand, F. Jam, M.R. Salimpour, The effect of porous insert position on the enhanced heat transfer in partially filled channel, Int. Communications in Heat and Mass Transfer 38 (2011) 1162-1167.

[13] H. Shokouhmand, F. Jam, M.R. Salimpour, Optimal porosity in an air heater conduit filled

with a porous matrix, Heat Transfer Engineering 30 (2009) 375–382.

[14] H. Shokouhmand, F. Jam, M.R. Salimpour, Simulation of laminar flow and convective heat transfer in conduits filled with porous media using Lattice Boltzmann method, Int. Communications Heat and Mass Transfer 36 (2009) 378–384.

[15] E. Ucar, M. Mobedi, I. Pop, Effect of an inserted porous layer located at a wall of a parallel plate channel on forced convection heat transfer, J. Transport in Porous Media (2013) 1-23, DOI 10.1007/s11242-013-0131-4.

[16] Y.T. Yang, M.L. Hwang, Numerical simulation of turbulent fluid flow and heat transfer characteristics in heat exchangers fitted with porous media, Int. J. Heat and Mass Transfer 52 (2009) 2956–2965.

[17] M.E. Nimvari, M. Maerefat, M.K. El-Hossaini, Numerical simulation of turbulent flow and heat transfer in a channel partially filled with a porous media, Int. J. Thermal Sciences 60 (2012) 131-141.

[18] K. Yang, K. Vafai, Analysis of heat flux bifurcation inside porous media incorporating inertial and dispersion effects – An exact solution, Int. J. Heat and Mass Transfer 54 (2011) 5286-5297.

[19] K. Yang, K. Vafai, Restrictions on the validity of the thermal conditions at the porous-fluid interface: an exact solution, ASME J. Heat Transfer 133 (2011c) 112601-1-112601-12.

[20] D. Jamet, M. Chandesris, On the intrinsic nature of jump coefficients at the interface between a porous medium and a free fluid region, Int. J. Heat Mass Transfer 52 (2009) 289–300.

[21] K. Vafai, R. Thiyagaraja, Analysis of flow and heat transfer at the interface region of a porous medium, Int. J. Heat Mass Transfer 30 (1987) 1391-1405.

[22] K. Vafai, S. Kim, Fluid Mechanics of the Interface Region Between a Porous Medium and a Fluid Layer—An Exact Solution, Int. J. Heat Fluid Flow 11 (1990) 254–256.

[23] A. Amiri, K. Vafai, T.M. Kuzay, Effects of boundary conditions on non-Darcian heat transfer through porous media and experimental comparisons, Numer. Heat Transfer, 27 Part A (1995) 651–664.

[24] B. Alazmi, K. Vafai, Constant wall heat flux boundary conditions in porous media under local thermal non-equilibrium conditions, Int. J. Heat Mass Transfer 45 (2002) 3071-3087.

[25] K. Yang, K. Vafai, Analysis of temperature gradient bifurcation in porous media – an exact solution, Int. J. Heat Mass Transfer 53 (2010) 4316–4325.

[26] Y. Mahmoudi, N. Karimi, Numerical investigation of heat transfer enhancement in a pipe

partially filled with a porous material under local thermal non-equilibrium condition, Int. J. Heat Mass Transfer 68 (2014) 161-173.

[27] C. Yang, K. Ando, A. Nakayama, A Local Thermal Non-Equilibrium Analysis of Fully Developed Forced Convective Flow in a Tube Filled with a Porous Medium, J. Transport in Porous Media 89 (2011) 237–249

[28] C. Yang, A. Nakayama, W. Liu, Heat transfer performance assessment for forced convection in a tube partially filled with a porous medium, Int. J. Thermal Sciences 54 (2012) 98-108.

[29] K. Vafai, K. Yang, A Note on Local Thermal Non-equilibrium in Porous Media and Heat Flux Bifurcation Phenomenon in Porous Media, J. Transport in Porous Media 96 (2013) 169–172.

[30] A. Marafie, K. Vafai, Analysis of non-Darcian effects on temperature differentials in porous media, Int. J. Heat Mass Transfer 44 (2001) 4401-4411.

[31] D.Y. Lee, K. Vafai, Analytical characterization and conceptual assessment of solid and fluid temperature differential in porous media, Int. J. Heat Mass Transfer 42 (1999) 423-435.

[32] P. Jiang, Z. Ren, Numerical investigation of forced convection heat transfer in porous media using a thermal non-equilibrium model, Int. J. of Heat and Fluid Flow 22 (2001) 102-110.

[33] G.J. Hwang, C.C. Wu, C.H. Chao, Investigation of non-Darcian forced convection in an asymmetrically heated sintered porous channel, J. of heat transfer 117 (1995) 725-732.

[34] O. Cekmer, M. Mobedi, B. Ozerdem, I. Pop, Fully Developed Forced Convection Heat Transfer in a Porous Channel with Asymmetric Heat Flux Boundary Conditions, J. Transport in Porous Media 53 (2010) 4316–4325.

[35] A. Amiri, K. Vafai, Analysis of dispersion effects and non thermal equilibrium, non-Darcian, variable porosity, in compressible flow through porous media, Int. J. Heat Mass Transfer 37 (1994) 939-954.

[36] B. Alazmi, K., Vafai, Analysis of Variants Within the Porous Media Transport Models, Journal of Heat Transfer 122 (2000) 303-326.

[37] W.-P. Breugem, The effective viscosity of a channel-type porous medium, Physics of Fluids, 19 (2007) 103104.

[38] R.C. Givler, S.A. Altobelli, A determination of the effective viscosity for the Brinkman–Forchheimer flow model, J. Fluid Mech. 258 (1994) 355–370.

[39] B.S. Al-Azmi, Analysis of transport models and computation algorithm for flow through porous media, PhD Thesis, Ohio State University, 2003.

[40] B. Alazmi, K. Vafai, Analysis of fluid flow and heat transfer interfacial conditions between a

porous medium and a fluid layer, Int. J. of Heat and Mass Transfer 44 (2001) 1735-1749.

[41] G.S. Beavers, D.D. Joseph, Boundary Conditions at a Naturally Permeable Wall, J. Fluid Mech. 30 (1967) 197–207.

[42] W.M. Rohsenow, J.P. Hartnett, Handbook of Heat Transfer, third ed., McGraw-Hill, New York, 1998.

[43] M. Kaviany, Principle of Heat Transfer in Porous Media, second ed., Spring-Verlag, New York, 1995.

[44] F.M. White, Fluid Mechanics, Fourth ed., McGraw-Hill, New York, 2006.

[45] O. Cekmer, M. Mobedi, B. Ozerdem, I. Pop, Fully Developed Forced Convection in a Parallel Plate Channel with a Centered Porous Layer, J. Transport in Porous Media 93 (2012) 179–201.

[46] F.P. Incropera, D.P. De Witt, T.L. Bergman, A.S. Lavine, Fundamental of heat and mass transfer, sixth ed., J. Wiley & Sons, New York, 2006.

[47] K.-H. Ko, N.K. Anand, Use of porous baffles to enhance heat transfer in a rectangular channel, Int. J. of Heat and Mass 46 (2003) 4191–4199.

1